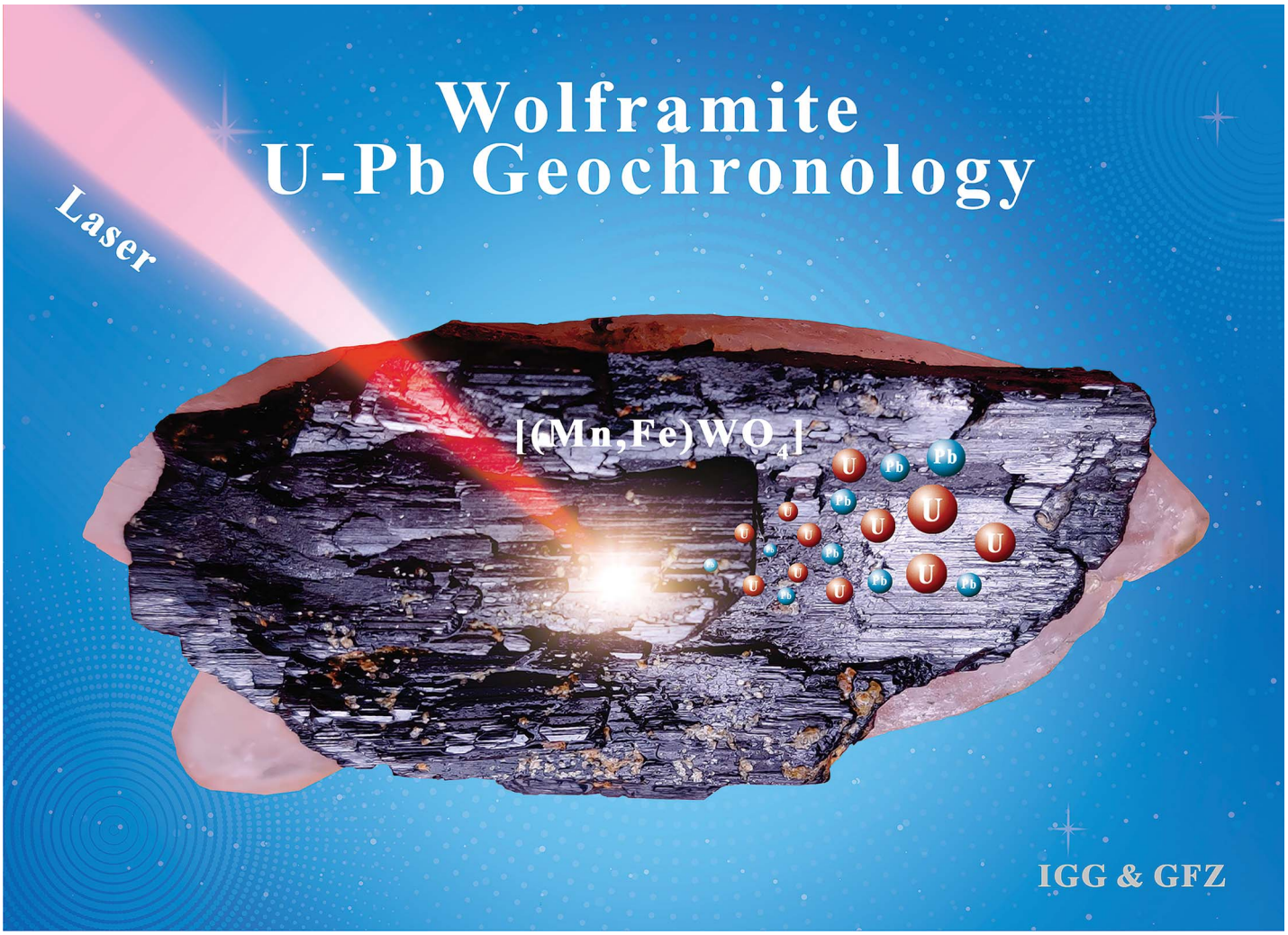

Showcasing research from Prof. Yue-Heng Yang, State Key Laboratory of Lithospheric Evolution, Institute of Geology and Geophysics, Chinese Academy of Sciences, Beijing, P.R.China.

Accurate and precise *in situ* U–Pb isotope dating of wolframite series minerals *via* LA-SF-ICP-MS

We present an analytical protocol for *in situ* U–Pb isotope dating of wolframite series minerals [(Fe,Mn)WO_4] by LA-SF-ICP-MS. The aim of this study is to establish a well-characterized U-Pb wolframite reference material for microanalysis, examine matrix effects between different wolframite end-members, estimate tungsten oxide interference on Hg and Pb using LA-ICP-MS, and estimate the closure temperature of wolframite as a reliable U-Pb geochronometer. Thus, it could be beneficial to get a better understanding of the geological conditions for the formation of tungsten mineralization.

As featured in:

See Yue-Heng Yang *et al.*, *J. Anal. At. Spectrom.*, 2020, **35**, 2191.

ROYAL SOCIETY OF CHEMISTRY

rsc.li/jaas

Registered charity number: 207890

JAAS

ROYAL SOCIETY OF CHEMISTRY

PAPER

View Article Online
View Journal | View Issue

Cite this: J. Anal. At. Spectrom., 2020, 35, 2191

Accurate and precise *in situ* U–Pb isotope dating of wolframite series minerals *via* LA-SF-ICP-MS†

Ming Yang,[abc] Yue-Heng Yang, *[abc] Shi-Tou Wu, [abc] Rolf L. Romer,[d] Xu-Dong Che,[e] Zi-Fu Zhao,[f] Wen-Sheng Li,[e] Jin-Hui Yang,[abc] Fu-Yuan Wu,[abc] Lie-Wen Xie, [abc] Chao Huang, [abc] Di Zhang[abc] and Yang Zhang[abc]

We present an analytical protocol for *in situ* U–Pb isotope dating of wolframite series minerals [(Fe,Mn)WO_4], the main ore mineral for tungsten, by LA-SF-ICP-MS. Precision and accuracy of the protocol was intensively assessed using our newly developed well-characterized U–Pb wolframite reference material. The tungsten oxide interference on Hg and Pb was investigated in detail. The matrix effect between ferberite and hübnerite during laser ablation was thoroughly examined for wolframite series minerals with a different Mn/(Mn + Fe) ratio. The closure temperature of wolframite, with respect to the U–Pb system, was evaluated. The application of eleven wolframite samples, with ages from ~1780 Ma to ~26 Ma, robustly demonstrated the feasibility of our approach. Most studied wolframite series minerals yielded U–Pb concordant or subconcordant ages. Samples with a relatively high U content and negligible common Pb content typically had a $^{206}Pb/^{238}U$ age precision of *ca.* 1%. The new *in situ* data agree well with published cassiterite or wolframite ages from the same locations. LA-SF-ICP-MS, with the advantages of high sensitivity, rapidity, and relatively low cost, as well as moderate spatial resolution (*i.e.*, 32 or 44 μm) that is sufficiently high to avoid sulfide inclusions, is the method of choice for *in situ* wolframite U–Pb microanalysis.

Received 21st May 2020
Accepted 6th August 2020

DOI: 10.1039/d0ja00248h

rsc.li/jaas

1. Introduction

Wolframite [(Fe,Mn)WO_4] forms an isomorphous solid-solution series between the iron-rich endmember ferberite [$FeWO_4$] and the manganese-rich endmember hübnerite [$MnWO_4$].[1] Tungsten is a critical resource because of its major and important applications in cutting tools as tungsten carbide, in the production of various steel grades as an alloying component, as filaments in light bulbs, and in the chemical industry, and also in military equipment.[2] Wolframite usually occurs in a wide variety of magmatic or hydrothermal ore deposits and is the dominant ore mineral of tungsten in granite-related W–Sn deposits.[3–5]

The improvement of exploration methods and, thus, the discovery of new tungsten deposits require a better understanding of the geological conditions for the formation of tungsten mineralization. Dating wolframite mineralization provides a critical step in linking the formation of W resources to the hydrothermal and magmatic history of an area. Several isotopic dating methods (*e.g.*, K(Ar)–Ar, Rb–Sr, Sm–Nd, Re–Os, and U–Pb) have been used to date ore minerals or paragenetically related gangue minerals and to determine the age of the mineralization processes. Among the various isotopic dating methods, the U–Pb method is generally considered to be the most powerful one to obtain precise and accurate ages because it includes two independent decay series and the concordance obtained by the two decay series provides (for geologically old samples) evidence for an undisturbed system.[6–11]

Wolframite minerals show a wide range of U contents (*e.g.*, <0.1 μg g^{-1} U to >100 μg g^{-1} U). The structure of wolframite does not favor the incorporation of common Pb during the crystallization of the mineral. Nonetheless, wolframite has variable contents of common Pb that are typically related to inclusions of minerals that do not exclude Pb. Depending on the U content, age, and content of initial Pb, the total Pb content in wolframite group minerals may be dominated by common Pb (<5% to >90%). Therefore, wolframite group minerals may not always be suitable for isotopic dating of bulk samples. There are few

[a]State Key Laboratory of Lithospheric Evolution, Institute of Geology and Geophysics, Chinese Academy of Sciences, Beijing 100029, China. E-mail: yangyueheng@mail.iggcas.ac.cn

[b]Innovation Academy of Earth Science, Chinese Academy of Sciences, Beijing 100029, China

[c]College of Earth and Planetary Sciences, University of Chinese Academy of Sciences, Beijing 100049, China

[d]GFZ German Research Centre for Geosciences, Telegrafenberg, 14473 Potsdam, Germany

[e]State Key Laboratory for Mineral Deposits Research, School of Earth Sciences and Engineering, Nanjing University, Nanjing 210046, China

[f]CAS Key Laboratory of Crust-Mantle Materials and Environments, School of Earth and Space Science, University of Science and Technology of China, Hefei, 230026, China

† Electronic supplementary information (ESI) available. See DOI: 10.1039/d0ja00248h

examples of successful U–Pb wolframite age determination by isotope dilution thermal ionization mass spectrometry (ID-TIMS).[12–16] The high precision of ID-TIMS U–Pb dating of wolframite minerals is offset by the delicate and time-consuming analytical protocol. Furthermore, the U–Pb TIMS dating of hydrothermal wolframite series minerals may be strongly affected by the presence of potentially abundant U and Pb bearing inclusions. For instance, inclusions of Pb-rich minerals (*e.g.*, scheelite, arsenopyrite, and pyrite) may overwhelm the Pb budget of wolframite with common Pb, making U–Pb dating impossible, whereas inclusions of U-rich minerals (*e.g.*, uraninite and columbite–tantalite) may dominate the U–Pb system of the wolframite bulk sample, eventually resulting in a situation where the U–Pb system of the inclusion determines the age of the bulk sample.[12–16] *In situ* U–Pb dating of wolframite using laser ablation inductively coupled plasma mass spectrometry (LA-ICP-MS) or an ion probe avoids many of these problems inherent to ID-TIMS that need a larger sample size. *In situ* U–Pb dating allows avoiding inclusions or altered domains and allows analysis of texturally different domains separately. Furthermore, sample preparation is relatively fast.[2,16–18] Isotopic dating by LA-ICP-MS or using an ion probe, however, requires access to well-characterized reference materials of known age.

Recently, Luo *et al.*[19,20] reported *in situ* U–Pb dating of wolframite by LA-ICP-MS, using the water vapor-assisted method and zircon as an external standard. As noted by Luo *et al.*,[20] the lack of matrix-matched wolframite reference materials is the major limitation for *in situ* U–Pb geochronological analysis.[21] Generally, *in situ* U–Pb isotope dating of minerals using a laser or ion probe requires matrix-matched reference materials to appropriately account for matrix effects. Despite the many potential significant uses of wolframite to study the formation of tungsten deposits, to our knowledge, there is no well-characterized reference material available for microanalysis. Moreover, the methodology of *in situ* U–Pb dating of wolframite *via* LA-ICP-MS or an ion probe (*e.g.*, isobaric interference, matrix effect, and closure temperature) has not been evaluated in detail.

Our collection of eleven wolframite samples, including ferberite and hübnerite endmembers and encompassing a broad range of formation ages, was selected from a much larger sample pool for this methodological investigation. The selected samples are those wolframite samples that in the first screening proved to be homogeneous and to have radiogenic Pb isotope compositions (using a high $^{206}Pb/^{208}Pb$ as proxy, as wolframite commonly has very low Th contents). This work has the following objectives: (1) establish a well-characterized U–Pb wolframite reference material for microanalysis; (2) examine matrix effects between hübnerite and ferberite during LA-ICP-MS; (3) estimate tungsten oxide interference on Hg and Pb for laser ablation; (4) estimate the closure temperature of wolframite as a reliable U–Pb geochronometer.

2. Experimental section

Eleven wolframite samples were separated by using a Frantz magnetic separator and were concentrated using heavy liquids. They were then selected by hand picking under a binocular microscope. Some separated grains were embedded in a 1 inch epoxy mount, sectioned to expose their interior, polished, and mapped by optical microscopy. Then chemical and isotopic homogeneity was investigated by electron microprobe analyses (EPMA) and laser ablation sector field ICP-MS (LA-SF-ICP-MS) analyses. Some relatively homogeneous samples were selected for U–Pb analysis by conventional ID-TIMS analysis. The detailed description of wolframite samples is provided in ESI† A1 to A4 (sample description), and only brief information is summarized in Table 1.

2.1 EPMA

EPMA were performed using a JEOL JXA-8100 instrument, located at the Institute of Geology and Geophysics, Chinese Academy of Sciences (IGGCAS), Beijing. The analytical conditions were: 20 nA current, 20 kV accelerating voltage, and 10 s counting time per element. The major element composition of wolframite samples is given in weight percent oxide (wt%). Wolframite samples range from hübnerite-rich ($MnWO_4$) to ferberite-rich ($FeWO_4$) compositions. The major elements of wolframite samples are provided in ESI Table S1.†

2.2 ID-TIMS

U–Pb dating of wolframite by ID-TIMS was performed at the GFZ German Research Centre for Geosciences, Potsdam, essentially using the analytical procedure described by Romer and Lüders.[12] To remove surface contamination the samples were rinsed in warm 1 M HNO_3, H_2O, and acetone. To remove sulfide inclusions abundant in some wolframite samples, the samples were ground in a mortar and leached in 3 M HNO_3. As this process also attacks wolframite, we modified the sample rinsing procedure to omit the 1 M HNO_3 step for most samples. After surface cleaning, a mixed ^{205}Pb–^{235}U tracer was added. The samples were dissolved in 40% HF on a hotplate at 160 °C for one day. While precipitation of tungstic oxide or metatungstate reduces the ion load on the column, precipitation before complete sample dissolution represents a problem as it may prevent complete homogenization of U and Pb from the sample and tracer. Therefore, an excess of HF was used for sample dissolution and all samples were inspected visually for absence of precipitates to ensure complete homogenization of the sample and tracer. Uranium and Pb were separated using ion exchange chemistry.[22] Uranium and Pb were loaded with H_3PO_4 and silica gel on separate Re single filaments. The isotopic ratios of U and Pb were measured using a Triton TIMS instrument operated in static or dynamic multi-collection mode using Faraday collectors and an ion counter, depending on the signal intensity. Lead was analyzed at 1200–1260 °C and U at 1300–1360 °C. Data reduction followed the procedures described by Schmid *et al.*[23] In particular, element concentrations, isotope ratios, ages and error estimates were calculated taking the following uncertainties into consideration: measurement errors, 30% uncertainty for the factor (*e.g.*, 0.1% amu^{-1}) used for the correction of instrumental mass fractionation, 50% uncertainty for the amount of Pb and U blank (here

Table 1 Information summary of wolframite investigated in this study[a]

Sample	Mineral	Location	Deposit type	Mineralization age/Ma	References
Bagge	Wolframite	Baggetorp W deposit, Sweden	Skarn type	Unkonwn	Kavari, 2018 [44]
Sewa	Wolframite	Unknown	Unkonwn	Unkonwn	—
MTM	Wolframite	Les Montmins, France	Vein type	334.4 ± 1.7 (Wol; U–Pb)	Harlaux *et al.*, 2018b [17]
Panasqueira	Ferberite	Panasqueira W–Sn–Cu deposit, Portugal	Vein type	320–280	Carocci *et al.*, 2018 [35]
Cornwall	Ferberite	Cornwall W–Sn deposit, United Kingdom	Vein/greisen type	283.2 ± 1.8 (Cst; U–Pb)	Neymark *et al.*, 2018 [10]
HTD	Hübnerite	Hamme Tungsten District, United States	Vein type	Unknown	—
YGX-2107	Wolframite	Yaogangxian W deposit, Hunan province, China	Vein type	159.1 & 153.7 (Wol; U–Pb)	Deng *et al.*, 2019 [18]
YGX-2113	Wolframite				
DP-12	Wolframite	Dangping W deposit, Jiangxi province, China	Vein type	180.8–154.9	Zhang *et al.*, 2012 [45]
XHS16	Wolframite	Xihuashan W deposit, Jiangxi province, China	Vein type	157.0 ± 2.5 (Mo; Re–Os)	Wang *et al.*, 2011 [46]
SHM	Hübnerite	Sweet Home Mine, United States	Vein type	25.7 ± 0.1 (Wol; U–Pb)	Romer and Lüders, 2006 [12]

[a] Wol: wolframite; Cst: cassiterite; Mo: molybdenite.

15 pg Pb and 1 pg U blank), and a compositional uncertainty for blank and initial Pb. In addition, an uncertainty of 0.3% was assigned to the $^{205}Pb/^{235}U$ ratio of the mixed isotopic tracer. Data reduction and error calculation were conducted by using Monte Carlo modeling of the measured data using the above uncertainty limits and allowing for error correlation when appropriate. Lead was corrected for blank and tracer Pb. The remaining ^{204}Pb was used for the correction of initial Pb. The composition of initial Pb was estimated from the data available for the corresponding region or for samples with relatively unradiogenic Pb isotope compositions using the $^{206}Pb/^{204}Pb$ *vs.* $^{238}U/^{204}Pb$ isochron diagram to determine initial $^{206}Pb/^{204}Pb$ and using the $^{207}Pb/^{204}Pb$ *vs.* $^{206}Pb/^{204}Pb$ diagram to determine initial $^{207}Pb/^{204}Pb$. Uncertainties in tables and the text are given at the 2σ level. The data were plotted using Isoplot v.3.23.[24]

2.3 LA-SF-ICP-MS

In situ U–Pb isotope measurements were performed using a single collector SF-ICP-MS instrument (Element XR, ThermoFisher) and a 193 nm ArF excimer laser (Geolas HD, Coherent), located at the IGGCAS. SF-ICP-MS analysis provides higher sensitivity and better precision than Quadrupole (Q)-ICP-MS analysis. Furthermore, SF-ICP-MS is more feasible to conduct U–Pb analysis at moderate spatial resolution. A detailed description of the instrumentation can be found in the report by Wu *et al.*[25,43] Helium and a little nitrogen were used as the carrier gas through the ablation cell and mixed with argon downstream of the ablation cell. Daily optimization of instrumental performance with NIST SRM 612 involved maximising the signal relative to background intensity ratios for Pb, Th and U, while satisfying low oxide production rates ($ThO^+/Th^+ < 0.5\%$), low double-charged ions ($Ca^{2+}/Ca^+ < 1.0\%$), and robust plasma conditions (sensitivity ratio of signal intensity, U^+/Th^+ in the range of 0.95–1.05). The isotopes ^{202}Hg, ^{204}Pb, ^{206}Pb, ^{207}Pb, ^{208}Pb, ^{232}Th, ^{235}U, and ^{238}U were analyzed by cycling of the electrostatic analyzer in the eScan mode, at a static magnetic mass. The dwell time was set to 15 ms for ^{206}Pb and ^{238}U, 2 ms for ^{202}Hg and ^{204}Pb, 10 ms for ^{208}Pb and ^{232}Th, and 30 ms for ^{207}Pb. The typical operating conditions are summarized in Table 2. Prior to each analytical session, a pre-ablation run was used to remove any contamination from the wolframite surface by ablating a 90 μm spot for 2 pulses. Each spot analysis consisted of an approximate 15 s background and 45 s sample data acquisition.

The raw data (sequence of calibration materials and samples and intensities of all isotopes of all scans) were exported for offline data reduction using Iolite software for semi-quantitative calculation of trace element contents[26] and Glitter software for U–Pb age calculation.[27] Signals of ^{204}Pb, ^{206}Pb, ^{207}Pb, ^{208}Pb, ^{232}Th, and ^{238}U were acquired for U–Pb dating, whereas the ^{235}U signal was calculated from ^{238}U on the basis of the ratio $^{238}U/^{235}U = 137.818$. YGX-2113 wolframite, used as a primary U–Pb reference material, showed a systematic elemental fractionation behavior, allowing for downhole fractionation correction. We analyzed Sewa or MTM wolframite as secondary reference materials to monitor data reproducibility. The mode of data reduction depended on the contribution of common Pb to the total amount of Pb present: (1) samples with low or no common Pb yield concordant data and, therefore, are reported as concordia dates; (2) samples with significant common Pb are reported as lower intercept dates in the Tera–Wasserburg diagram. In addition, weighted $^{206}Pb/^{238}U$ mean dates were calculated using the ^{207}Pb correction of common Pb,[28] assuming a common Pb composition corresponding to the two-stage crustal Pb model of Stacey and Kramers.[29–31] The U–Pb ages and weighted mean ages were calculated using the Isoplot 3.23 software package.[24]

3. Results

The individual U–Pb isotope data of wolframite samples are provided in the ESI in Table S2† (individual *in situ* U–Pb data). The ID-TIMS U–Pb analytical results for wolframite are shown in Table 3, while the compilation of the U–Pb LA-SF-ICP-MS dating results is shown in Table 4.

3.1 ID-TIMS U–Pb geochronology

Three wolframite samples were selected for ID-TIMS U–Pb analysis. Wolframite samples YGX-2113 and YGX-2107 from the

Table 2 Typical LA-SF-ICP-MS instrumental conditions

Laser ablation system	
Manufacturer, model & type	Coherent, Geolas HD
Ablation cell & volume	In-house built cell, aerosol dispersion volume <3 cm^3
Laser wavelength	193 nm
Pulse width	20 ns
Energy density/fluence	~4 J cm^{-2}
Repetition rate	5 Hz
Spot size	32, 44, 60, 90 μm
Sampling mode/pattern	Single hole drilling, two cleaning pulses
Ablation gas flow	~0.75 L min^{-1} (He)
Ablation duration	45 seconds
SF-ICP-MS	
Manufacturer, model & type	ThermoFisher Scientific Element XR
RF power	~1340 W
Guard electrode	Connected (Pt)
Sample cone	Nickel Jet sample cone
Skimmer cone	Nickel "X" version skimmer cone
Coolant gas flow (Ar)	15.00 L min^{-1}
Auxiliary gas flow (Ar)	0.80 L min^{-1}
Carrier gas flow (Ar)	0.95 L min^{-1}
Enhancement gas flow (N_2)	8 mL min^{-1}
Scan mode	E-scan
Isotopes measured (m/z) + sample time	^{202}Hg (2 ms), ^{204}Pb (2 ms), ^{206}Pb (15 ms), ^{207}Pb (30 ms), ^{208}Pb (10 ms), ^{232}Th (10 ms), ^{235}U (10 ms), and ^{238}U (15 ms)
Mass window	20%
Sample per peak	20
Detection system	Single SEM detector in triple mode, counting, analog and Faraday
Resolution ($M/\Delta M$)	Low (~300)
Total integration time per reading	0.27 s

Yaogangxian W deposit are hübneritic wolframite, with broad ranges of Mn/(Mn + Fe) of 0.29 to 0.88 for YGX-2113 and 0.47 to 0.74 for YGX-2107 (Fig. 1). Sample YGX-2113 has a relatively high and homogeneous U content of 20.3 to 38.1 μg g^{-1} and relatively high radiogenic Pb isotope compositions. The $^{206}Pb/^{204}Pb$ value of YGX-2113 varies from to 313.6 to 1145. Apparent $^{206}Pb/^{238}U$ ages of the five wolframite fractions range from 158.6 ± 0.6 Ma to 163.5 ± 1.2 Ma (Table 3). Fraction 13Y4, which has the least radiogenic Pb isotope composition, falls above the concordia line. This fraction has several times higher common Pb contents than the other fragments from the same sample, which may be related to inclusion of sulfide minerals. The position of this sample in the concordia diagram may be related to such Pb_{common} bearing inclusions. Fraction 13Y1 falls below the concordia line. The remaining analyses of sample YGX-2113 yield a concordia age of 160.9 ± 0.2 Ma (2σ, $n = 4$, MSWD = 0.5) and a weighted mean $^{206}Pb/^{238}U$ age of 160.9 ± 0.7 Ma (2σ, $n = 4$) (Fig. 2a).

Five fragments from the Sewa sample were analyzed. Sewa is a ferberitic wolframite with a Mn/(Mn + Fe) ranging from 0.16–0.31 (Fig. 1). $^{206}Pb/^{204}Pb$ values of individual fragments fall in the range from 90.1 to 147.3. The amounts of 491 to 1336 pg common Pb correspond to initial Pb contents of 0.72 to 1.08 μg g^{-1}. Thus, common Pb contributes 35 to 50% to the Pb budget of these samples. The apparent $^{206}Pb/^{238}U$ ages of the five wolframite fractions range from 725.9 ± 7.8 to 792.5 ± 11.3 Ma (2σ). The lower apparent ages are related to samples that are clearly discordant. The three samples with the highest $^{206}Pb/^{204}Pb$ and concordant yield $^{206}Pb/^{238}U$ ages overlapping within error in the range from 786.7 to 792.5 Ma. These three samples yield a concordia age of 791.4 ± 2.1 Ma (2σ, $n = 3$, MSWD = 2.7), which coincides with the weighted mean $^{206}Pb/^{238}U$ age of 789.1 ± 9.5 Ma (2σ, $n = 3$) (Fig. 2b).

Sample YGX-2107, which was collected from the same W deposit as sample YGX-2113, shows $^{206}Pb/^{204}Pb$ values ranging from 303.5 to 533.4 (Table 3). Using the same initial Pb isotope composition as for sample YGX-2113 for common Pb correction, all the analysis results of YGX-2107 fall below the concordia (light-colored ellipses in Fig. 2c). The apparent $^{206}Pb/^{238}U$ age of these discordant samples ranges from 156.4 ± 0.8 Ma to 167.7 ± 1.0 Ma, *i.e.*, some of these apparent ages are higher than the age of the granite.[18] To test whether this anomalous data pattern is due to the common Pb correction, we plotted the data in a $^{206}Pb/^{204}Pb$ *vs.* $^{238}U/^{204}Pb$ diagram. The six wolframite samples fall on a straight line that yields an isochron age of 155.9 ± 9.6 Ma (2σ, MSWD = 47; Fig. 2d) and a very high initial $^{206}Pb/^{204}Pb$ = 43.0 ± 0.4 (2σ, MSWD = 47). The corresponding $^{207}Pb/^{204}Pb$ and $^{208}Pb/^{204}Pb$ ratios (Table 3) were estimated using the correlation among the Pb isotope compositions of the various samples. Using this radiogenic initial Pb isotope composition (Table 3) reduces the apparent $^{206}Pb/^{238}U$ and $^{207}Pb/^{235}U$ ages and shifts most wolframite data onto the concordia in the $^{206}Pb/^{238}U$ *vs.* $^{207}Pb/^{235}U$ diagram. Fraction 7Y3 falls below the concordia and, therefore, was not taken into consideration. Fractions 7Y1 and 7Y2 yield lower apparent ages than the other fractions, including those from sample YGX2113

Table 3 ID-TIMS U–Pb analytical dated in this study

Sample[a]	Weight (mg)	Concentrations (μg g^{-1}) U	Pb	^{206}Pb/^{204}Pb measured ratio[b]	Com. lead (pg)	Radiogenic Pb[c] (at%) ^{206}Pb	^{207}Pb	^{208}Pb
YGX-2107, Hunan province, China								
^{206}Pb/^{204}Pb = 43.0 ± 1.0, ^{207}Pb/^{204}Pb = 16.9 ± 0.1, ^{208}Pb/^{204}Pb = 39.5 ± 0.5								
7Y1	0.564	16.6	0.41	455.3	22	94.58	4.67	0.75
7Y2	0.557	19.6	0.54	303.5	61	94.99	4.64	0.36
7Y3	0.426	20.7	0.49	533.4	13	94.39	4.83	0.78
7Y4	0.488	21.4	0.55	442.3	31	94.87	4.67	0.46
7Y5	1.155	12.9	0.34	486.6	48	94.67	4.68	0.65
7Y6	0.635	20.5	0.55	433.4	47	94.69	4.70	0.61
YGX-2113, Hunan province, China								
^{206}Pb/^{204}Pb = 18.8 ± 0.2, ^{207}Pb/^{204}Pb = 15.8 ± 0.1, ^{208}Pb/^{204}Pb = 39.4 ± 0.5								
13Y1	0.769	34.4	0.83	761.4	39	95.18	4.74	0.09
13Y2	0.515	20.3	0.50	480.2	19	95.26	4.65	0.09
13Y3	0.512	25.6	0.68	323.4	52	95.15	4.68	0.17
13Y4	1.182	33.3	0.94	313.6	202	95.38	4.61	0.02
13Y5	0.545	21.6	0.54	438.6	22	94.81	4.69	0.51
13Y6	0.741	38.1	0.90	1145	22	94.99	4.67	0.34
Sewa, Rwanda								
^{206}Pb/^{204}Pb = 22.6 ± 1.0, ^{207}Pb/^{204}Pb = 15.9 ± 0.1, ^{208}Pb/^{204}Pb = 39.5 ± 1.0								
S1	1.165	8.9	1.85	123.0	898	93.42	6.28	0.30
S2	1.234	12.2	2.53	113.2	1336	92.59	6.39	1.02
S3	0.510	11.7	2.26	116.8	491	92.70	6.54	0.76
S4	0.557	7.4	1.84	90.1	524	93.47	6.31	0.21
S5	0.916	10.6	1.98	147.3	664	93.91	6.09	—

Sample[a]	Atomic ratios[c] ^{206}Pb/^{238}U	2σ (%)	^{207}Pb/^{235}U	2σ (%)	^{207}Pb/^{206}Pb	2σ (%)	Rho	Apparent ages[d] (Ma) ^{206}Pb/^{238}U	2σ	^{207}Pb/^{235}U	2σ	^{207}Pb/^{206}Pb	2σ
YGX-2107, Hunan province, China													
^{206}Pb/^{204}Pb = 43.0 ± 1.0, ^{207}Pb/^{204}Pb = 16.9 ± 0.1, ^{208}Pb/^{204}Pb = 39.5 ± 0.5													
7Y1	0.0243	1.32	0.1652	1.66	0.0493	0.91	0.84	154.7	2.0	155.3	2.4	163.5	21.2
7Y2	0.0240	1.32	0.1616	2.18	0.0489	1.67	0.65	152.8	2.0	152.1	3.1	141.9	39.3
7Y3	0.0243	1.32	0.1717	1.70	0.0512	1.01	0.80	155.0	2.0	160.9	2.5	249.5	23.2
7Y4	0.0249	1.19	0.1688	2.01	0.0492	1.55	0.64	158.3	1.9	158.4	3.0	158.8	36.3

Table 3 (*Contd.*)

	Atomic ratios[c]							Apparent ages[d] (Ma)					
Sample[a]	$^{206}Pb/^{238}U$	2σ (%)	$^{207}Pb/^{235}U$	2σ (%)	$^{207}Pb/^{206}Pb$	2σ (%)	Rho	$^{206}Pb/^{238}U$	2σ	$^{207}Pb/^{235}U$	2σ	$^{207}Pb/^{206}Pb$	2σ
7Y5	0.0253	1.39	0.1722	2.23	0.0494	1.64	0.68	160.8	2.2	161.3	3.8	167.8	38.3
7Y6	0.0253	1.10	0.1731	1.41	0.0496	1.26	0.82	161.2	1.7	162.1	2.1	175.4	19.0
YGX-2113, Hunan province, China													
$^{206}Pb/^{204}Pb = 18.8 \pm 0.2$, $^{207}Pb/^{204}Pb = 15.8 \pm 0.1$, $^{208}Pb/^{204}Pb = 39.4 \pm 0.5$													
13Y1	0.0249	0.38	0.1709	0.94	0.0498	0.85	0.43	158.6	0.6	160.2	1.4	183.3	20.0
13Y2	0.0253	0.41	0.1698	2.75	0.0488	2.69	0.23	160.8	0.6	159.3	4.0	136.1	63.2
13Y3	0.0250	0.65	0.1696	2.05	0.0492	1.91	0.37	159.1	1.0	159.1	3.0	158.9	45.0
13Y4	0.0257	0.76	0.1712	1.28	0.0483	0.99	0.63	163.5	1.2	160.4	1.9	114.7	24.0
13Y5	0.0253	0.39	0.1726	0.86	0.0494	0.76	0.48	161.2	0.6	161.7	1.3	168.5	17.7
13Y6	0.0253	0.37	0.1719	0.45	0.0492	0.26	0.82	161.3	0.6	161.1	0.7	157.4	6.0
Sewa, Rwanda													
$^{206}Pb/^{204}Pb = 22.6 \pm 1.0$, $^{207}Pb/^{204}Pb = 15.9 \pm 0.1$, $^{208}Pb/^{204}Pb = 39.5 \pm 1.0$													
S1	0.1305	1.11	1.2102	2.10	0.0672	2.19	0.18	790.9	8.3	805.3	11.7	845.4	45.6
S2	0.1264	1.23	1.2026	2.21	0.0690	2.27	0.22	767.1	8.9	801.8	12.3	899.6	47.0
S3	0.1192	1.13	1.1596	2.15	0.0706	2.28	0.14	725.9	7.8	781.7	11.7	944.7	46.7
S4	0.1308	1.51	1.2182	2.38	0.0676	2.72	0.07	792.5	11.3	808.9	13.3	854.9	56.5
S5	0.1298	0.90	1.1612	1.74	0.0649	1.80	0.19	786.7	6.7	782.5	9.5	770.5	38.0

[a] Small fragments from single wolframite crystals were selected. All fragments show fresh fracture surfaces. Samples were analyzed at the GFZ German Research Centre for Geosciences, Potsdam, Germany. [b] Lead isotope ratios were corrected for 0.1% amu^{-1} fractionation, blank, and isotopic tracer. Concentrations of Pb and U were determined using a ^{205}Pb–^{235}U mixed isotope tracer. Total blanks were less than 15 pg for lead and less than 1 pg for uranium. [c] Lead corrected for fractionation, blank, isotopic tracer, and initial lead. Uncertainties of blank and initial Pb, as well as fractionation and $^{205}Pb/^{235}U$ of tracer were propagated onto the isotope ratios. [d] Apparent ages were calculated using the constants of Jaffey *et al.* (1971)[47] recommended by IUGS: $\lambda_{238} = 1.55125 \times 10^{-10}\ y^{-1}$, $\lambda_{235} = 9.848 \times 10^{-10}\ y^{-1}$.

Table 4 Compilation of the U–Pb LA-SF-ICP-MS dating results of wolframite investigated in this study

Wolframite	n	Pb (μg g^{-1}) (2SD)	Th (μg g^{-1}) (2SD)	U (μg g^{-1}) (2SD)	Th/U (2SD)	^{238}U/^{206}Pb Mean	^{238}U/^{206}Pb 2SD	^{207}Pb/^{206}Pb Mean	^{207}Pb/^{206}Pb 2SD	^{207}Pb/^{235}U Mean	^{207}Pb/^{235}U 2SD	^{206}Pb/^{238}U Mean	^{206}Pb/^{238}U 2SD	f_{206} [a] (%) Mean	f_{206} [a] (%) 2SD	207 Corr. age (Ma) ^{206}Pb/^{238}U Mean	207 Corr. age (Ma) ^{206}Pb/^{238}U 2SD	ID-TIMS age
Bagge	12	2.57 (1.57)	2.11 (11.9)	7.94 (5.24)	0.218 (1.196)	3.09	0.06	0.1177	0.0336	5.4340	1.7716	0.3231	0.0060	1.42	3.69	1784	42	
Sewa	16	3.29 (1.99)	0.45 (0.19)	22.21 (12.31)	0.021 (0.010)	7.46	0.11	0.0862	0.0019	1.6052	0.0568	0.1340	0.0020	2.51	3.87	791.5	12.8	791.4 (2.1)[d]
MTM	16	1.33 (1.12)	0.02 (0.04)	28.38 (21.01)	0.001 (0.001)	18.79	0.26	0.0528	0.0079	0.3852	0.0463	0.0532	0.0007	0.16	0.76	334.4	5.8	334.4 (1.7)[b]
Panasqueira	17	0.11 (0.16)	0.004 (0.01)	2.26 (2.39)	0.002 (0.002)	20.14	1.20	0.0533	0.0122	0.3575	0.0145	0.0497	0.0028	0.34	1.00	312.3	19.7	
Cornwall	16	0.79 (1.64)	0.13 (0.04)	13.66 (5.37)	0.010 (0.001)	22.01	0.59	0.0552	0.0110	0.3341	0.0405	0.0454	0.0013	0.51	1.14	285.3	10.6	
HTD	18	0.61 (1.47)	0.01 (0.01)	14.04 (35.28)	0.001 (0.002)	22.12	0.35	0.0644	0.0221	0.3855	0.1280	0.0452	0.0007	1.56	2.76	280.7	4.0	
YGX-2107	19	0.76 (1.52)	0.50 (0.90)	32.83 (66.14)	0.016 (0.013)	39.52	0.84	0.0503	0.0060	0.1738	0.0107	0.0253	0.0005	0.22	0.60	160.9	4.1	160.1 (1.1)[d]
YGX-2113	17	0.48 (0.60)	0.19 (0.21)	20.27 (22.03)	0.010 (0.004)	39.75	0.71	0.0513	0.0051	0.1729	0.0049	0.0252	0.0004	0.27	0.59	159.8	3.3	160.9 (0.2)[d]
DP-12	19	1.37 (2.44)	0.54 (0.95)	60.84 (113.7)	0.009 (0.005)	39.45	1.25	0.0490	0.0053	0.1738	0.0113	0.0254	0.0008	0.12	0.40	161.4	5.6	
XHS16	20	0.24 (0.35)	0.17 (0.26)	10.24 (16.02)	0.018 (0.009)	39.47	0.70	0.0522	0.0080	0.1777	0.0119	0.0253	0.0004	0.41	0.91	160.7	3.3	
SHM	14	0.15 (0.20)	0.12 (0.32)	35.47 (49.46)	0.003 (0.008)	248.03	8.65	0.0561	0.0174	0.0318	0.0107	0.0040	0.0001	1.23	2.14	25.6	0.6	25.7 (0.3)[c]

[a] f_{206}, common ^{206}Pb in total ^{206}Pb; $f_{206} = [(^{207}\text{Pb}/^{206}\text{Pb})\text{total} - (^{207}\text{Pb}/^{206}\text{Pb})\text{radiogenic}]/[(^{207}\text{Pb}/^{206}\text{Pb})\text{init} - (^{207}\text{Pb}/^{206}\text{Pb})\text{radiogenic}]$. [b] ID-TIMS age: ID-TIMS concordia age from Harlaux *et al.* (2018a).[15] [c] ID-TIMS age: ID-TIMS ^{206}Pb/^{238}U age from Romer and Lüders (2006).[12] [d] ID-TIMS age: this study.

Fig. 1 Major element composition of the eleven wolframite samples dated in this study. The variation in Mn/(Fe + Mn) shows the compositional range between the manganese-rich endmember hübnerite and the iron-rich endmember ferberite.

from the same deposit and, therefore, were not taken into consideration either. Using the radiogenic initial Pb isotope composition, estimated from the isochron diagram, yields a concordia age of 160.1 ± 1.1 Ma (2σ, $n = 3$, MSWD = 1.8) and a weighted average age of 160.1 ± 2.2 Ma (2σ, $n = 3$). This result agrees well with the age of sample YGX-2113 (Fig. 2a), which is from the same deposit. The anomalous initial Pb isotope composition of sample YGX-2107 indicates that initial Pb within a deposit may not be homogeneous and may be relatively radiogenic if rocks or minerals with radiogenic Pb have been leached by the mineralizing fluid. It is important to note that such interaction of the mineralizing fluid with the wall rocks implies that Pb in the fluid is derived from a different source and, thus, may be heterogeneous if the various contributions to Pb have different isotopic compositions. Furthermore, minerals that precipitate from such a fluid also may be initially heterogeneous. Especially for samples with important contributions of common Pb to the Pb budget, such an initial heterogeneity also results in a scatter of the data in the various Pb–Pb and U–Pb diagrams. A similar case of the anomalously radiogenic initial Pb phenomenon has been documented for a wolframite sample from the St-Goussaud deposit.[15] In that study, Pb from fluid inclusions in quartz associated with wolframite confirmed that the mineralizing fluid had a radiogenic initial Pb isotope composition. The radiogenic composition of common Pb in wolframite YGX-2107 and in wolframite from the St-Goussaud deposit may be related to fluid or mineral inclusions in wolframite. If wolframite and its inclusions are not cogenetic, their initial Pb isotope composition, however, may be different.

3.2 Laser ablation U–Pb dating of wolframite

The wolframite sample Bagge was collected from the Baggetrop tungsten deposit in the Bergslagen region, south central

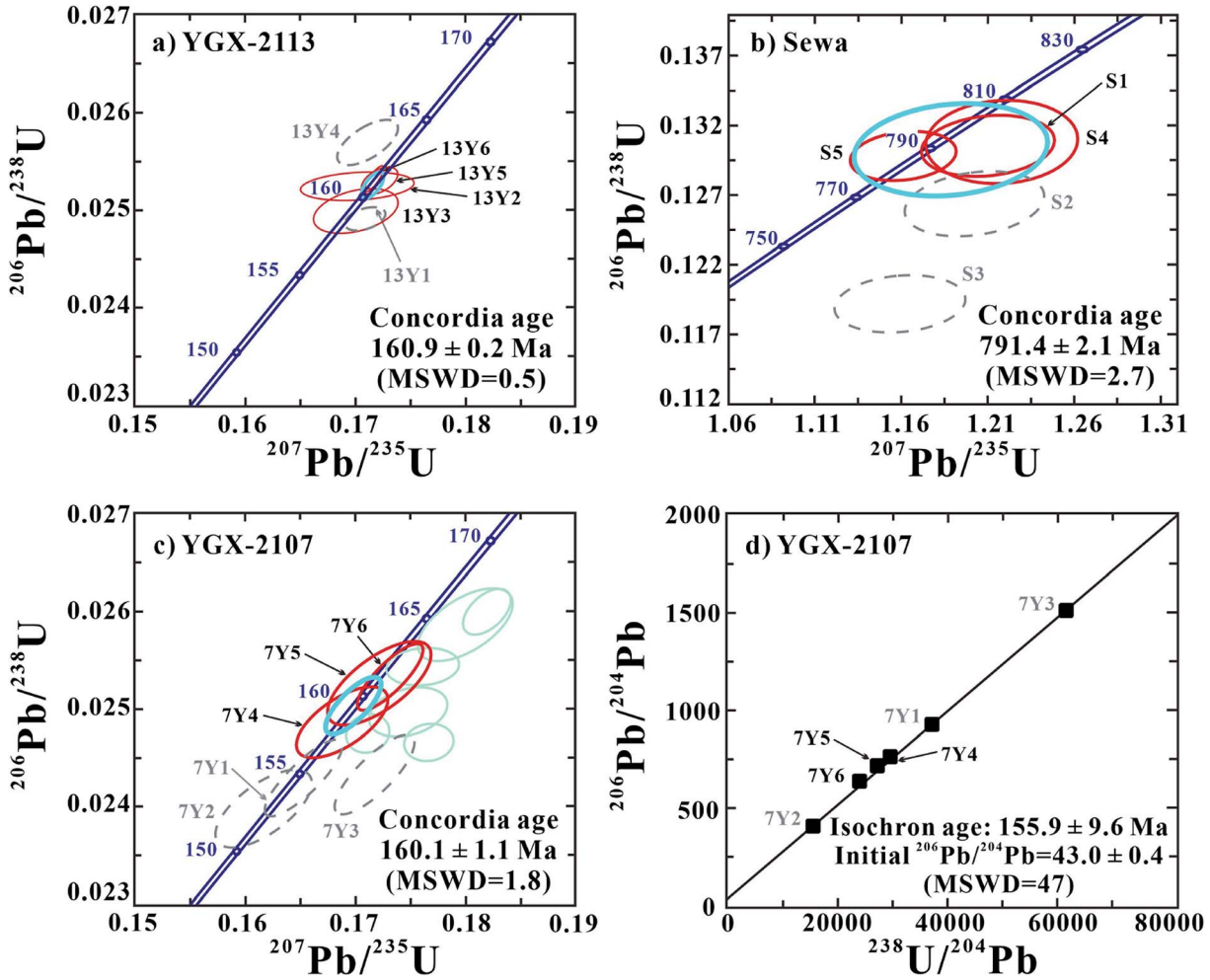

Fig. 2 (a–c) Concordia diagrams for ID-TIMS data for wolframite samples YGX-2113 (Yaogangxian), Sewa (Rwanda), and YGX-2107 (Yaogangxian). Samples shown with dashed lines are not used for calculation of the weighted concordia age. (d) $^{206}Pb/^{204}Pb$–$^{238}U/^{204}Pb$ isochron diagram for YGX-2107 (Yaogangxian). Diagrams and ages were calculated using ISOPLOT (Ludwig, 2003).[24]

Sweden. The dated sample is a ferberitic wolframite with a Mn/(Mn + Fe) ranging from 0.15 to 0.51 and an average U content of 7.94 ± 5.24 μg g^{-1} (2σ, n = 12). The measured f_{206} ranges from 0 to 5.3%. All twelve analyses are clustered near the concordia line, yielding a lower intercept age of 1791 ± 17 Ma (2σ, n = 12, MSWD = 0.6) in a Tera–Wasserburg diagram, consistent with the ^{207}Pb corrected weighted mean $^{206}Pb/^{238}U$ age of 1786 ± 20 Ma (2σ) (Fig. 3a). This result agrees well with the ID-TIMS titanite age of 1789 ± 2 Ma (2σ) for another tungsten deposit in the region[32] and the ID-TIMS columbite age of 1789 ± 2 Ma (2σ) for a close by rare-element pegmatite.[33]

The wolframite sample Sewa (Rwanda) has U concentrations ranging from 10.63 to 35.10 μg g^{-1}. The f_{206} of laser ablation spot analyses ranges from 0.4% to nearly 20%. For comparison, the common Pb contribution to the bulk fractions from the same wolframite sample ranges from 35% to 50%. The ^{207}Pb-corrected weighted average $^{206}Pb/^{238}U$ age of 791.8 ± 6.3 Ma for sixteen LA-ICP-MS analyses (Fig. 3b) is in good agreement with the ID-TIMS U–Pb wolframite age (Fig. 2b). The lower intercept age for the wolframite sample Sewa in the Tera–Wasserburg diagram is 791.6 ± 6.0 Ma (2σ, n = 16, MSWD = 0.1).

The wolframite sample MTM from the French Massif Central is a ferberitic wolframite with an average Mn/(Mn + Fe) of 0.25. The U content ranges from 16.72 to 44.80 μg g^{-1}. The average f_{206} composition is 0.16 ± 0.76% (2σ, n = 16). Sixteen MTM wolframite analyses yielded a concordia age of 333.6 ± 1.6 Ma (2σ, MSWD = 0.1; Fig. 3c), which is consistent with the ID-TIMS age of 334.6 ± 1.7 Ma (2σ, n = 3)[15] and the LA-ICP-MS age of 333.3 ± 1.0 Ma (2σ, n = 53).[20]

The wolframite sample YGX-2107 has U, Th, and Pb contents of 32.83 ± 66.14, 0.50 ± 0.90, and 0.76 ± 1.52 μg g^{-1}, respectively. The average f_{206} is 0.22 ± 0.60%. The LA-SF-ICP-MS U–Pb data are concordant and yield an age of 161.3 ± 0.8 Ma (2σ, n = 19, MSWD = 0.7, Fig. 3d), which is in good agreement with the ID-TIMS age of YGX-2107 and YGX-2113.

The wolframite samples of XHS16 (Xihuashan) and DP-12 (Dangping), Jiangxi Province, Southern China, show very low f_{206}, *i.e.*, they have very low contents of common Pb. Both samples have variable U contents, ranging from 2.33 to 38.02 μg

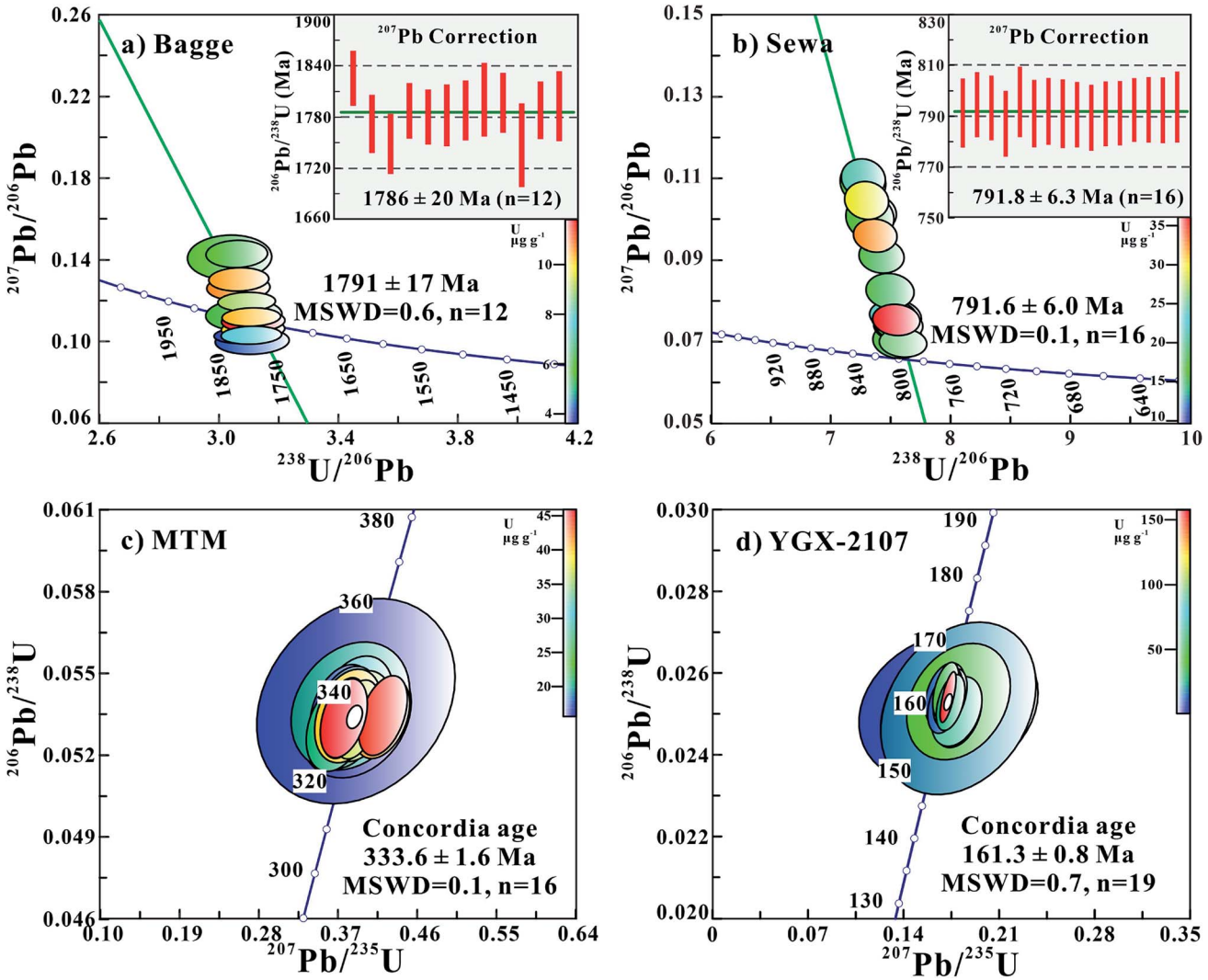

Fig. 3 LA-SF-ICP-MS U–Pb data of wolframite. (a and b) Tera–Wasserburg diagram and (c and d) concordia diagram for wolframite samples Bagge (Sweden), Sewa (Rwanda), MTM (France), and YGX-2107 (China), respectively. Data were plotted and evaluated using ISOPLOT (Ludwig, 2003).[24]

g^{-1} (XHS16) and 16.57 to 250.10 μg g^{-1} (DP-12). Our *in situ* analyses yielded concordant U–Pb ages of 160.7 ± 0.9 Ma (2σ, n = 20, MSWD = 1.4) for XHS16 and 161.0 ± 0.7 Ma (2σ, n = 19, MSWD = 0.3) for DP-12 (Fig. 4). These ages agree well with the narrow age span for granitic magmatism with related W–Sn mineralization, as indicated for instance by zircon and cassiterite LA-ICP-MS U–Pb ages of 159.5 Ma to 159.8 Ma for the Piaotang W–Sn deposit in this district.[33]

3.3 Laser ablation U–Pb dating of ferberite

The ferberite samples Panasqueira and Cornwall are from the Panasqueira W–Sn–Cu deposit, Central Portugal, and a W–Sn deposit associated with the Tregonning granite, southwest England, respectively. In spite of its relatively low U content, spot analyses of the Panasqueira sample yield a concordant U–Pb age of 313.3 ± 3.2 Ma (2σ, n = 17, MSWD = 0.1) (Fig. 5a), which is within the range of the rutile U–Pb age of 305.2 ± 5.7 Ma for the Panasqueira deposit.[34] Similarly, spot analyses of the ferberite sample Cornwall yield a concordia U–Pb age of 286.2 ± 1.5 Ma (2σ, n = 16, MSWD = 0.8) (Fig. 5b), which is in good agreement with the ^{207}Pb-corrected ^{206}Pb/^{238}U cassiterite age of 283.2 ± 1.8 Ma (2σ, n = 60, MSWD = 1.4) and the age range of 270 to 295 Ma for spatially associated granites of the Cornubian ore field.[10,36]

3.4 Laser ablation U–Pb dating of hübnerite

The sample HTD from the Hamme Tungsten District, North Carolina, United States, is nearly pure hübnerite (Fig. 1). It has a relatively low f_{206} (1.56 ± 2.76%). All data clusters are near the concordia line and yield a lower intercept age of 281.3 ± 2.4 Ma in the Tera–Wasserburg diagram (2σ, n = 18, MSWD = 0.1), consistent with a ^{207}Pb corrected weighted mean ^{206}Pb/^{238}U age of 281.2 ± 2.5 Ma (2σ, n = 18) (Fig. 6a). The hübnerite sample SHM was collected from the Sweet Home Mine (Alma,

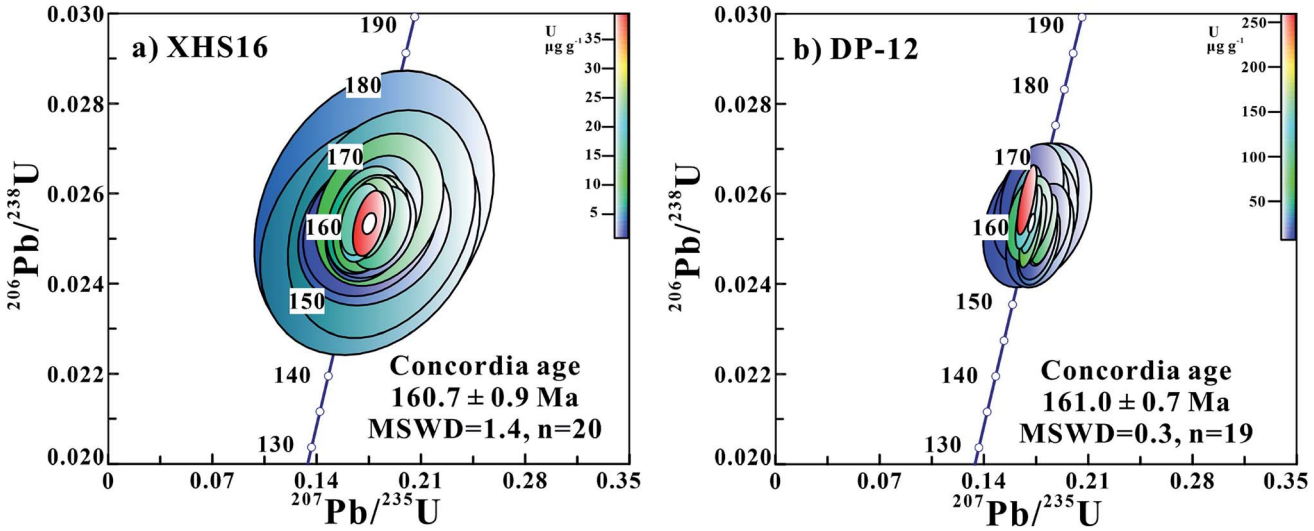

Fig. 4 U–Pb concordia diagrams for LA-SF-ICP-MS U–Pb data of wolframite samples XHS16 (a) and DP-12 (b) from Jiangxi province, Southern China. Data were plotted and evaluated using ISOPLOT (Ludwig, 2003).[24]

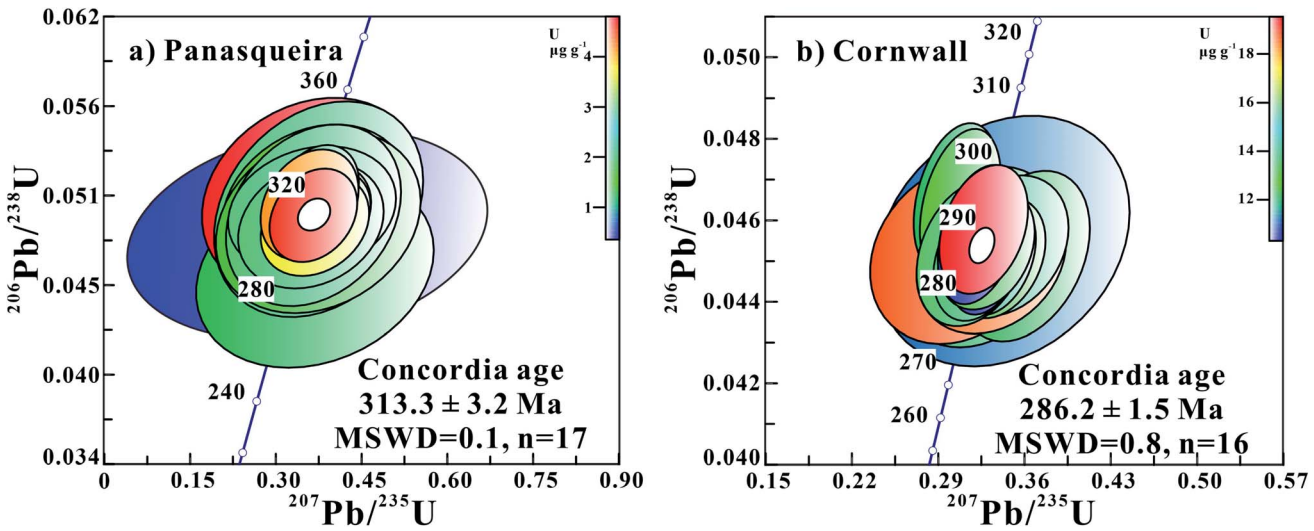

Fig. 5 U–Pb concordia diagrams for ferberite samples from Panasqueira (Central Portugal) (a) and Cornwall (United Kingdom) (b). Data were plotted and evaluated using ISOPLOT (Ludwig, 2003).[24]

Colorado). Our LA-SF-ICP-MS data yield an intercept age of 25.7 ± 0.4 Ma (2σ, $n = 14$, MSWD = 0.3) in the Tera–Wasserburg diagram and a $^{206}Pb/^{238}U$ age of 25.7 ± 0.3 Ma (2σ, $n = 14$), after ^{207}Pb correction (Fig. 6b). The $^{206}Pb/^{238}U$ ID-TMS age of aliquots of the same crystal is 25.7 ± 0.3 Ma (2σ, $n = 3$).[12]

4. Discussion

4.1 Closure temperature of wolframite

Wolframite is generally stable over a large range of temperatures and pressures (300–900 °C and 0.5–2 kbar) and under hydrothermal conditions over a large range of fO_2 values.[37] Nevertheless, little information is available about the stability of the U–Pb isotope system in wolframite and therefore about its reliability for U–Pb dating.[15] The closure temperature of wolframite with respect to the U–Pb system has not been evaluated earlier. Petrographic observations indicate that the mineral is susceptible to alteration during later stages of hydrothermal activity. Such alteration could disturb and reset the original U–Pb isotope system. Fig. 7 shows the calculated temperature of closure for Pb in wolframite based on the methods of Zhao and Zheng.[38] Note that wolframite has a Pb closure temperature of 900–1000 °C for grains with a size of 100 μm at cooling rates of 10–200 °C Ma^{-1}, indicating that the temperature of closure for Pb in wolframite is considerably higher than the temperature at which tungsten mineralization typically forms. For instance, fluid inclusion microthermometry studies show that most hydrothermal tungsten deposits formed at medium to low temperatures of 100 °C to 500 °C.[3,9,39–41] Hence, the age of unaltered wolframite dates the

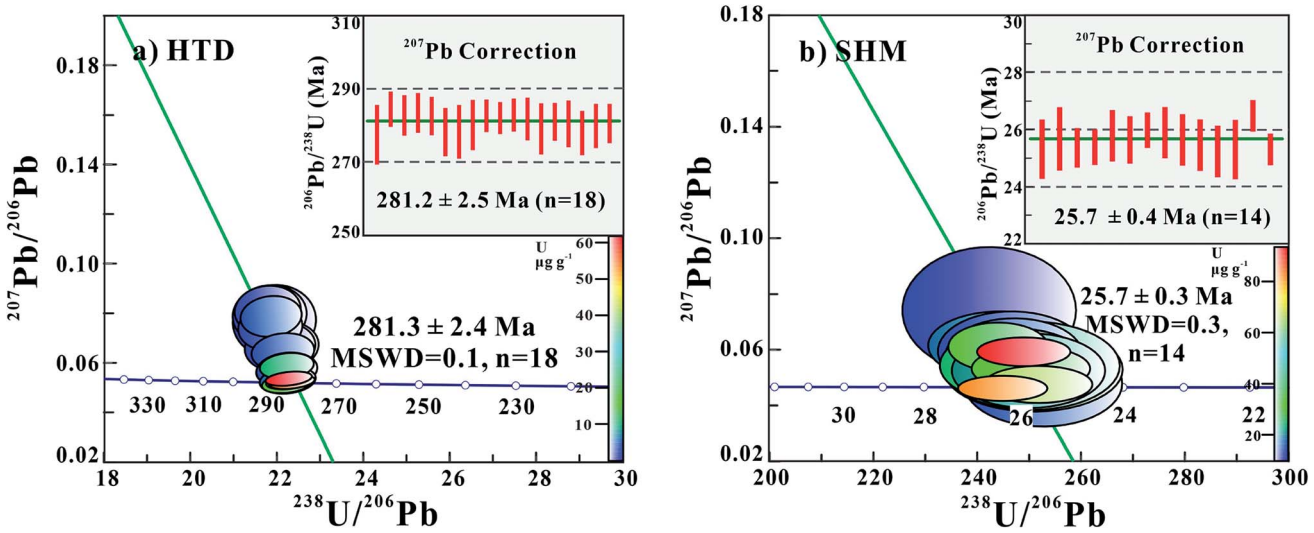

Fig. 6 Terra–Wasserburg diagrams for hübnerite samples HTD (a) and SHM (b) from the United States. Data were plotted and evaluated using ISOPLOT (Ludwig, 2003).[24]

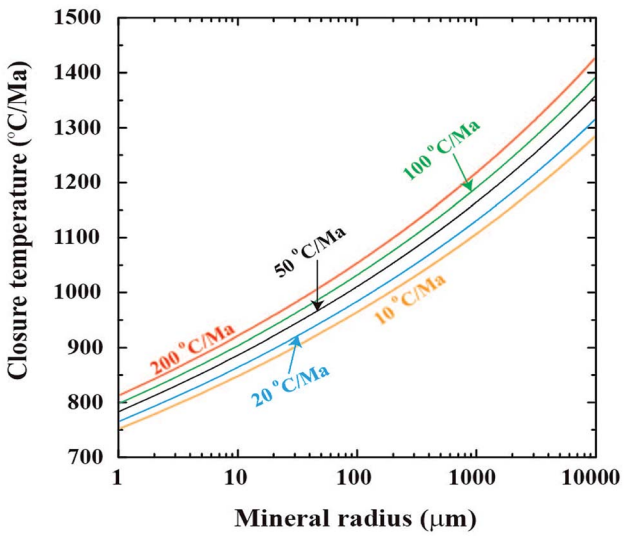

Fig. 7 Calculation of Pb closure temperatures in wolframite based on the methods of Zhao and Zheng (2007).[38]

time of wolframite formation rather than later isotopic closure. Thus, unaltered wolframite may be as a reliable U–Pb chronometer as cassiterite,[10,11] which is in line with the consistence of U–Pb wolframite and cassiterite age data from the same W–Sn deposit (see the example above).

4.2 Tungsten oxide interference

As shown in Fig. 8, there is serious and significant tungsten oxide interference of $^{186}W^{16}O$ and $^{184}W^{18}O$ on ^{202}Hg during laser ablation of the wolframite sample YGX-2113. Furthermore, there is also some memory effect of tungsten oxide, observable even after the laser is turned off (Fig. 8b). The wolframite sample YGX-2113 has no or negligible common Pb and, therefore, the interference of $^{186}W^{18}O$ (red diamond) on ^{204}Hg and ^{204}Pb can be observed (Fig. 8b). Samples with appreciable contents of common Pb also will experience this interference, but it is not possible to quantify the contribution of the interference. Thus, the ^{204}Pb correction procedure for common Pb contribution is not feasible for *in situ* U–Pb dating of wolframite by LA-ICP-MS. For U–Pb dating of wolframite by Secondary Ion Mass Spectrometry (SIMS) using oxygen as the primary ion source, the ^{204}Pb correction procedure is not feasible either. The alternative correction procedures, *i.e.*, ^{207}Pb and ^{208}Pb correction,[42] should be preferentially used. For minerals with very low Th contents, for instance cassiterite (typically Th/U < 10^{-4} to 10^{-5}),[10,11] ^{208}Pb correction may be the method of choice. For wolframite that has a relatively low to moderate Th/U ratio of 10^{-2} to 10^{-3} (Table S2†) ^{207}Pb correction may be preferable. For wolframite with significant common Pb contribution either correction procedure may be impracticable and the best age estimate is obtained from the intercept age in the Tera–Wasserburg diagram.

4.3 Matrix effect between ferberite and hübnerite

The composition of wolframite [(Fe,Mn)WO_4] represents an isomorphous solid-solution series between the iron-rich endmember ferberite [$FeWO_4$] and the manganese-rich endmember hübnerite [$MnWO_4$]. Because of the similar atomic mass of the substituting elements, Mn (55) and Fe (56), and the insignificant contribution of other elements, no matrix effect due to composition is expected between the endmembers ferberite and hübnerite. This is indirectly confirmed by our observations. Using sample YGX-2113 as the wolframite reference material, the LA-SF-ICP-MS U–Pb ages of ferberite (Fig. 5) and hübnerite (Fig. 6) agree with known ages from the corresponding deposits.

4.4 U–Pb wolframite reference material

The ideal U–Pb reference material is characterized by relatively high U and low common Pb, as well as low variance of their U–Pb ratios. Nevertheless, a material with uniform U–Pb ratios was

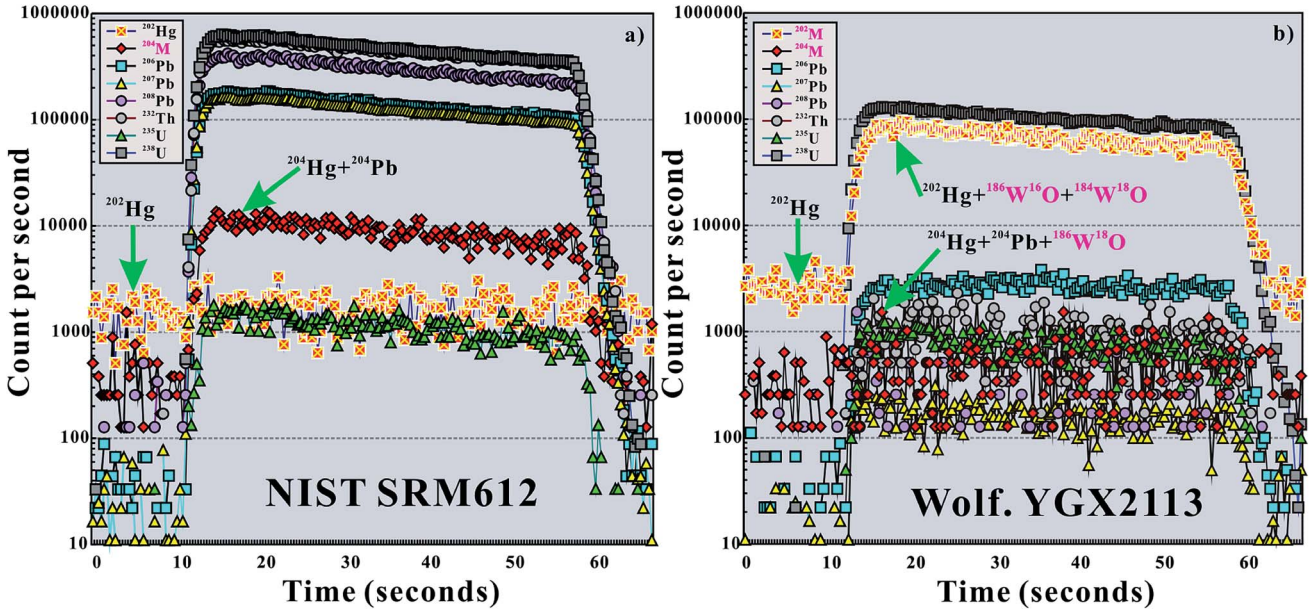

Fig. 8 Time *vs.* signal sensitivity for a typical LA-SF-ICP-MS analysis of (a) the reference material NIST SRM612 and (b) wolframite YGX-2113.

not easily found.[7,8,10,11] Among the wolframite samples investigated here, the wolframite sample YGX-2113 produces consistently concordant analyses and shows a low contribution of common Pb (Fig. 2a). Furthermore, wolframite YGX-2113 has relatively high and homogeneous U contents and, therefore, is highly suited to serve as the *in situ* primary reference material. The wolframite samples Bagge and Sewa have variable U contents (Table 4) and variable contributions of common Pb, which result in slightly variable ^{207}Pb/^{206}Pb (Fig. 3). Because of this heterogeneity, the wolframite samples Bagge and Sewa are little suited to be primary standards, but they represent useful secondary standards to check the data quality during each analytical session. Similarly, the wolframite samples Panasqueira, Cornwall, YGX-2107, and SHM are useful samples for U–Pb quality control, in particular for Mesozoic and Tertiary wolframite samples. The wolframite samples DP-12 and XHS16 have very low common Pb contents and plot in tight clusters in the concordia diagram (Fig. 4). They may become the primary wolframite reference material for U–Pb dating once their age is confirmed.

5. Conclusions

We established an analytical protocol for *in situ* U–Pb dating of wolframite series minerals by LA-SF-ICP-MS. The precision and accuracy of the present protocol has been validated by U–Pb dating using the ID-TIMS technique for some wolframite reference materials suitable for LA-SF-ICP-MS dating. There are serious and significant interference of tungsten oxide (^{186}W^{16}O and ^{184}W^{18}O on ^{202}Hg; ^{186}W^{18}O on ^{204}Hg and ^{204}Pb) on Hg and Pb, and therefore, the ^{204}Pb correction is not applicable for wolframite U–Pb dating using *in situ* methods, such as LA-SF-ICP-MS or SIMS. Variations in the Mn/(Mn + Fe) ratio do not affect the observed matrix effect, which implies that the same reference material can be used for the dating of ferberite and hübnerite. The calculated closure temperature for the U–Pb system of wolframite is higher than the formation temperature of hydrothermal tungsten mineralization. Wolframite U–Pb LA-SF-ICP-MS ages ranging from ~1790 Ma to ~26 Ma agree well with ID-TIMS ages for the same samples, U–Pb ages for cassiterite from the same W–Sn deposit, or published ages for rocks associated with the tungsten deposits. Concordant or subconcordant U–Pb ages are obtained for wolframite series minerals with negligible common Pb contents at a precision of *ca.* 1% for wolframite series minerals with a relatively high U content. LA-SF-ICP-MS dating of wolframite series minerals has the advantages of high sensitivity, rapidity and relatively low cost, as well as moderate spatial resolution (*i.e.*, 32 or 44 μm),[43] and is more preferable. As wolframite is easily altered by late fluids and may have abundant inclusions, such as Pb-bearing sulfide minerals, which are hard to avoid in bulk sample analysis, *in situ* analysis by LA-SF-ICP-MS may become the method of choice for wolframite U–Pb age determination.

Conflicts of interest

The authors declare no competing financial interest.

Acknowledgements

This study was financially supported by the Natural Science Foundation of China (No. 41525012) and the German government BMBF-r4 grant 033R134A awarded to RLR. We are indebted to Dr Tao Luo, Tony Nikischer, Prof. Ru-Cheng Wang, and Prof. Pei Ni for providing wolframite samples. We are grateful to editor Alice Smallwood and the reviewers Prof. Xiao-Ping Xia and Prof. Ryan Ickert for the thoughtful comments. We are also thankful to Prof. Zhu-Yin Chu for the insightful

suggestions and Yao Li for the mass spectrometric measurements.

References

1 R. L. Romer and U. Kroner, *Gondwana Res.*, 2016, **31**, 60–95.
2 H. E. Gäbler, W. Schink, S. Goldmann, A. Bahr and T. Gawronski, *J. Forensic Sci.*, 2017, **62**, 881–888.
3 S. A. Wood and I. M. Samson, *Econ. Geol.*, 2000, **95**, 143–182.
4 P. Černý, P. L. Blevin, M. Cuney and D. London, *Econ. Geol.*, 2005, **100**, 337–370.
5 R. J. King, *Geol. Today*, 2005, **21**, 33–37.
6 G. E. Gehrels, V. Valencia and J. Ruiz, *Geochem., Geophys., Geosyst.*, 2008, **9**, Q03017.
7 S. Seman, D. F. Stockli and N. M. McLean, *Chem. Geol.*, 2017, **460**, 106–116.
8 Y. H. Yang, F. Y. Wu, Q. L. Li, Y. Rojas-Agramonte, J. H. Yang, Y. Li, Q. Ma, L. W. Xie, C. Huang, H. R. Fan, Z. F. Zhao and C. Xu, *Geostand. Geoanal. Res.*, 2019, **43**, 543–565.
9 H. Legros, J. Mercadier, J. Villeneuve, R. L. Romer, E. Deloule, M. V. Lichtervelde, S. Dewaele, P. Lach, X. D. Che, R. C. Wang, Z. Y. Zhu, E. Gloaguen and J. Melleton, *Chem. Geol.*, 2019, **512**, 69–84.
10 L. A. Neymark, C. S. Holm-Denoma and R. J. Moscati, *Chem. Geol.*, 2018, **483**, 410–425.
11 P. A. Carr, M. D. Norman and V. C. Bennett, *Chem. Geol.*, 2017, **467**, 122–133.
12 R. L. Romer and V. Lüders, *Geochim. Cosmochim. Acta*, 2006, **70**, 4725–4733.
13 K. Pfaff, R. L. Romer and G. Markl, *Eur. J. Mineral.*, 2009, **21**, 817–836.
14 P. Lecumberri-Sanchez, R. L. Romer, V. Lüeders and R. J. Bodnar, *Miner. Deposita*, 2014, **49**, 353–369.
15 M. Harlaux, R. L. Romer, J. Mercadier, C. Morlot, C. Marignac and M. Cuney, *Miner. Deposita*, 2018a, **53**, 21–51.
16 H. Legros, M. Harlaux, J. Mercadier, R. L. Romer, M. Poujol, A. Camacho, C. Marignac, M. Cuney, R. C. Wang, N. Charles and M. Y. Lespinasse, *Ore Geol. Rev.*, 2020, **117**, 103302.
17 M. Harlaux, J. Mercadier, C. Marignac, C. Peiffert, C. Cloquet and M. Cuney, *Chem. Geol.*, 2018b, **479**, 58–85.
18 X. D. Deng, T. Luo, J. W. Li and Z. C. Hu, *Chem. Geol.*, 2019, **515**, 94–104.
19 T. Luo, Z. C. Hu, W. Zhang, Y. S. Liu, K. Zong, L. Zhou, J. F. Zhang and S. Hu, *Anal. Chem.*, 2018, **90**, 9016–9024.
20 T. Luo, X. D. Deng, J. W. Li, Z. C. Hu, W. Zhang, Y. S. Liu and J. F. Zhang, *J. Anal. At. Spectrom.*, 2019, **34**, 1439–1446.
21 T. W. Tang, K. Cui, Z. Zheng, J. F. Gao, J. J. Han, J. H. Yang and L. Liu, *Gondwana Res.*, 2020, **83**, 217–231.
22 R. L. Romer, W. Heinrich, B. Schröder-Smeibidl, A. Meixner, C. O. Fischer and C. Schulz, *Contrib. Mineral. Petrol.*, 2005, **149**, 400–429.
23 R. Schmid, R. L. Romer, L. Franz, R. Oberhänsli and G. Martinotti, *J. Metamorph. Geol.*, 2003, **21**, 531–538.
24 K. R. Ludwig, *Isoplot 3.23*, 2003, vol. 3, pp. 1–70.
25 S. Wu, G. Wörner, K. P. Jochum, B. Stoll, K. Simon and A. Kronz, *Geostand. Geoanal. Res.*, 2019, **43**, 567–584.
26 C. Paton, J. Hellstrom, B. Paul, J. Woodhead and J. Hergt, *J. Anal. At. Spectrom.*, 2011, **26**, 2508–2518.
27 W. L. Griffin, W. J. Powell, N. J. Pearson and S. Y. O'Reilly, *Mineralogical Association Canada Short Course*, 2008, vol. 40, pp. 308–311.
28 M. S. A. Horstwood, J. Kosler, G. Gehrels, S. E. Jackson, N. M. McLean, C. Paton, N. Peason, K. Sircombe, P. Sylvester, P. Vermeesch, J. F. Bowring, D. J. Condon and B. Schoene, *Geostand. Geoanal. Res.*, 2016, **40**, 311–332.
29 J. S. Stacey and J. D. Kramers, *Earth Planet. Sci. Lett.*, 1975, **26**, 207–221.
30 D. M. Chew, J. A. Petrus and B. S. Kamber, *Chem. Geol.*, 2014, **363**, 185–199.
31 Y. H. Yang, F. Y. Wu, J. H. Yang, R. H. Mitchell, Z. F. Zhao, L. W. Xie, C. Huang, Q. Ma, M. Yang and H. Zhao, *J. Anal. At. Spectrom.*, 2018, **33**, 231–239.
32 R. L. Romer and B. Öhlander, *GFF*, 1994, **116**, 161–166.
33 R. L. Romer and S. A. Smeds, *Precambrian Res.*, 1997, **82**, 85–99.
34 R. Q. Zhang, J. J. Lu, B. Lehmann, C. Y. Li, G. L. Li, L. P. Zhang, J. Cuo and W. D. Sun, *Ore Geol. Rev.*, 2017, **82**, 268–284.
35 E. Carocci, C. Marignac, M. Cathelineau, F. Pinto and L. Truche, Le stade, in *Proceedings of the 24th Réunion des Sciences de la Terre*, Lille, France, 22–26, October 2018, p. 439.
36 W. D. Smith, J. R. Darling, D. S. Bullen, S. Lasalle, I. Pereira, H. Moreira, C. J. Allen and S. Tapster, *Lithos*, 2019, **336**, 14–26.
37 X. D. Che, R. L. Linnen, R. C. Wang, A. Aseri and Y. Thibault, *Geochim. Cosmochim. Acta*, 2013, **106**, 84–98.
38 Z. F. Zhao and Y. F. Zheng, *Am. Mineral.*, 2007, **92**, 289–308.
39 K. Rickers, R. Thomas and W. Heinrich, *Miner. Deposita*, 2006, **41**, 229–245.
40 R. Thomas, P. Davidson and H. Beurlen, *Mineral. Petrol.*, 2012, **106**, 55–73.
41 N. Hulsbosch, M. C. Boiron, S. Dewaele and P. Muchez, *Geochim. Cosmochim. Acta*, 2016, **175**, 299–318.
42 T. R. Ireland and I. S. Williams, *Rev. Mineral. Geochem.*, 2003, **53**, 215–241.
43 S. T. Wu, M. Yang, Y. H. Yang, L. W. Xie, C. Huang, H. Wang and J. H. Yang, *Int. J. Mass Spectrom.*, 2020, **456**, 116394.
44 P. Khavari, Master's thesis, Luleå University of Technology, 2018, pp. 6–15.
45 W. L. Zhang, R. M. Hua, R. C. Wang, L. Xie and X. D. Che, *Miner. Deposits*, 2012, **31**, 633–634.
46 F. Y. Wang, C. Y. Li, M. X. Ling, H. Zhang, Y. L. Sun and W. D. Sun, *Resource Geol.*, 2011, **61**, 414–423.
47 A. H. Jaffey, K. F. Flynn, L. E. Glendenin, C. Bentley and A. M. Essling, *Phys. Rev.*, 1971, **C4**, 1889–1906.

Sample description

A1. Wolframite from Sweden (Bagge), Rwanda (Sewa), France (MTM), and China (YGX-2107, YGX-2113)

Wolframite sample Bagge was collected from the Baggetorp deposit near Tjällmo in the southwestern part of the Bergslagen region, south central Sweden. This mine was shut down after the Second World War due to the drop in tungsten and fluorite price (Khavari, 2018). The age of this mineralization is not known. The regional geological development provides the following age constraints: The rocks of the Bergslagen ore province formed during the Svecofennian orogeny and were intruded along the western and southern margin of this province by rocks of the Transscandinavian Granite-Porphyry Belt (Ohlsson, 1979). There are three main periods of magmatic activity in the Svecofennian domain: Early Svecofennian (1.85-1.89 Ga) volcano sedimentary supracrustal units, Early Svecofennian (1.85-1.89 Ga) plutonic bodies, and Late Svecofennian (ca. 1.80-1.78 Ga) granites (Andersson et al., 2006). These events in part overlap with magmatic events in the Transscandinavian Granite-Porphyry Belt, which includes geochemically distinctive 1.82-1.75 Ga and 1.73-1.65 Ga old magmatic rocks (Andersson et al., 2004). Within the Bergslagen ore province there are several granite-related tungsten deposits, among which the Yxsjöberg tungsten-skarn deposit is the most important one. Romer and Öhlander (1994) obtained a U-Pb titanite age of 1789 ± 2 Ma (2σ) for the Yxsjöberg deposit using isotope dilution thermal ionization mass spectrometry (ID-TIMS). There are numerous rare element pegmatites in the southern part of the Bergslagen ore province, most importantly ca. 1.80-1.82 Ga old NYF (Niobium-Yttrium-Fluorine) pegmatites and ca. 1.80-1.75 Ga old LCT (Lithium-Cesium-Tantalum) pegmatites (Romer and Smeds, 1997). Skrupetorp, the LCT-type pegmatite closest to the Baggetorp pegmatite, yields a U-Pb columbite age of 1786 ±1 Ma (2σ) (Romer and Smeds, 1997). The ages of the Yxsjöberg tungsten deposit and the Skrumpetorp pegmatite possibly give the best expectation values for the age of the Baggetorp pegmatite.

Sample Sewa is a ferberitic wolframite, and the exact location of Sewa is unknown, but it probably originates from Rwanda.

Sample MTM originates from Les Montmins, a granite-related hydrothermal W ± Sn deposits in the French Massif Central. Wolframite from this location had been studied by Harlaux et al. (2018a; 2018b) for U-Pb age and fluid inclusions. MTM wolframite has a very large range of U contents and the crystallization age constrained by ID-TIMS is 334.4 ± 1.7 Ma (2σ, MSWD = 3.6) (Harlaux et al., 2018a). Luo et al. (2019) used the water vapor-assisted LA-ICP-MS U-Pb dating method and obtained a lower intercept age of 333.3 ± 1.0 Ma in the Tera-Wasserburg diagram.

Wolframite samples YGX-2107 and YGX-2113 were collected from the Yaogangxian tungsten deposit, Hunan Provence, South China. Both samples are hübneritic wolframite. The Yaogangxian tungsten deposit is one of the numerous W deposits in the Nanling metallogenic belt. In this region, W mineralization commonly occurs within the granites and/or extends into the Paleozoic wall rocks. Fluid inclusion studies demonstrate that the area was affected by several mineralization events (e.g., Legros et al. 2020). Isotopic dating of ore and gangue minerals, including $^{40}Ar/^{39}Ar$ dating of muscovite and, Re-Os dating of molybdenite, and U–Pb dating of hydrothermal zircon, cassiterite, and wolframite suggest that W mineralization and multiple overprints of the mineralization occurred between 170 Ma and 133 Ma (e.g., Wang et al., 2008; Wang et al., 2009; Hu et al., 2012; Wang and Ren, 2018; Deng et al., 2019; Legros et a., 2020). The Yaogangxian deposit is a granite-related vein-type W deposit (Peng et al., 2006; Zhao et al., 2017). The granites had been dated between 170.7 ± 1.5 Ma and 152.7 ± 1.8 Ma by zircon U–Pb dating (Che et al., 2009; Wang et al., 2009; Li et al., 2011; Dong et al., 2014). Recently, Deng et al. (2019) dated the wolframite from Yaogangxian deposit by LA-ICP-MS, using a non-matrix-matched water-vapor assisted method, and distinguished

early and late wolframite domains. The two texturally defined domains yielded U-Pb ages of 159.1 ± 2.0 Ma (2σ; MSWD=0.7) and 153.7 ± 0.7 Ma (2σ; MSWD=0.5), respectively.

A2. Wolframite from Jiangxi province (XHS16, DP-12), south China

Wolframite sample XHS16 is from the Xihuashan tungsten deposit, which is a vein-type deposit genetically associated with the Xihuashan granite pluton that is located in the Nanling metallogenic belt, southeastern China. Magmatic rocks in this region typically are 180 Ma to 150 Ma old (Sun, 2006; Zhou et al., 2006; Li et al., 2007; Wang et al., 2011; Li et al., 2013; Zhang et al., 2017) and, thus, tungsten mineralization related to these rocks should fall in a similar age range (Mao et al., 2007; Hua et al., 2008; Guo et al., 2011; Wang et al., 2011; Mao et al., 2013). Wang et al. (2011) reported a Re–Os isochron age of 157.0 ± 2.5 Ma (2σ) for molybdenite intergrown with wolframite in the oldest generation of the Xihuashan pluton. This age is in good agreement with the LA-ICP-MS U–Pb zircon age of 155.7 ± 2.2 Ma (2σ).

Wolframite sample DP-12 is from the Dangping tungsten deposit in the Nanling region. Magmatic rocks in this region dominantly include Yanshanian granitic complexes (Zhang et al., 2012). Zhang et al. (2012) that yield U-Pb zircon ages of 180.8 Ma to 154.9 Ma, i.e., which falls in the same age range as the 180 Ma to 150 Ma Xihuashan granitic complex (Sun, 2006; Zhou et al., 2006; Li et al., 2007; Wang et al., 2011; Li et al., 2013; Zhang et al., 2017).

A3. Ferbrite from Portugal (Panasqueira) and the United Kingdom (Cornwall)

The Panasqueira W–Sn–Cu ore deposit, one of the largest tungsten deposits in Western Europe, is located in the Variscan Central Iberian Zone (CIZ) in north-central Portugal. Several generations of voluminous granitoids intruded the CIZ during the late stages of the Variscan orogeny (320–280 Ma), The Panasqueira mineralization is genetically associated with the greisen cupola of one of these granites, the Panasqueira granite, that is exposed in the deepest part of the mine (Foxford et al. 2000; Jacques et al., 2015; Carocci et al., 2018). The age of the Panasqueira deposit is not well known. From the regional context, it should be younger than ca. 320 Ma, i.e., the older generation of post-kinematic granites, and older than 288 Ma, i.e., the age of last-stage muscovite (Snee et al., 1988).

The ferberite sample named Cornwall was collected from a tin and copper deposit associated with the Tregonning-Godolphin Granite that formed during the late stages of the Variscan orogeny (Neymark et al., 2018; Smith et al., 2019; Moscati and Neymark, 2020). The granitic plutons of the Cornubian Batholith were intruded from ~ 295 to 270 Ma (Smith et al., 2019; Moscati and Neymark, 2020). Neymark et al. (2018) reported the U-Pb age of a cassiterite sample from a deposit related to the Tregonning granite to be 283.2 ± 1.8 Ma, which agrees with the age range known for Cornubian granites of the Cornubian ore field (Smith et al., 2019).

A4. Hübnerite from the United States (HTD, SHM)

The hübnerite sample HTD is from the Hamme Tungsten District, which includes a series of steeply dipping quartz wolframite veins in the Piedmont of North Carolina, United States (Foose et al., 1980). The tungsten-bearing quartz veins are concentrated along the western contact between the Vance County granite and late Precambrian to early Paleozoic slates and phyllite (Foose et al., 1980). Granitic rocks similar to the Vance County pluton yielded Rb-Sr and U-Pb ages ranging from 520 to 620 Ma (Fullagar, 1971; Glover and Sinha, 1973). Foose et al. (1980) demonstrated that the Hamme Tungsten District had experienced at least two episodes of folding and shearing. The entire area has been overprinted by the 300-280 Ma Alleghenian orogeny.

The hübnerite sample SHM was collected from the Sweet Home Mine located in the Alma mining district on the eastern slope of central Colorado's Mosquito Range. The deposit originally has been mined for silver, but is best known for its gem-quality rhodochrosite. Late stage hübnerite forms blade-crystals that are intergrown with quartz Similar rhodochrosite-hübnerite veins are spatially related with Teritay porphyry-type molybdenum mineralization, including the nearby world-class deposits of Climax and Henderson (Seedorff and Einaudi, 2004; Lüders et al., 2009). Romer and Lüders (2006) analyzed three Sweet Home Mine hübnerite fragments from a single crystal and reported a $^{206}Pb/^{238}U$ age of 25.7 ± 0.3 Ma, which is consistent with the $^{40}Ar/^{39}Ar$ ages from sericite ranging from 26.1 ± 0.1 and 25.5 ± 0.1 Ma (Barbá et al. 2005).

References

1. K. E. Barbá, E. P. Nelson, D. Misantoni, M. W. Hitzman, P. W. Layer, *In: Rhoden HN, Steininger RC and Vikre PG (eds) Geol Soc Nevada Symp*, 2005, 698–708.
2. E. Carocci, C. Marignac, M. Cathelineau, F. Pinto, L. Truche, *In Proceedings of the 24th Réunion des Sciences de la Terre, Lille, France*, 22–26 October 2018, 439.
3. X. D. Che, R. C. Wang, W. L. Zhang, J. C. Zhu, J. J. Lu, L. Xie, A. P. Yu, *Bull. Mineral. Petrol. Geochem.*, 2009, **28**, 467 (In Chinese).
4. X. D. Deng, T. Luo, J. W. Li, Z. C. Hu, *Chem. Geol.*, 2019, **515**, 94–104.
5. S. Dong, X. Bi, R. Hu, Y. Chen, *Acta Petrol. Sin.*, 2014, **30**, 2749–2765 (In Chinese with English abstract).
6. M. P. Foose, J. F. Slacka, T. Casadevall, *Econ. Geol.*, 1980, **75**, 515–522.
7. K. A. Foxford, R. Nicholson, D. A. Polya, R. P. B. Hebblethwaite, *J. Struct. Geol.*, 2000, **22**, 1065–1086.
8. P. D. Fullagar, *Geol. Soc. America Bull.*, 1971, **82**, 2845–2862.
9. L. Glover, A. K. Sinha, *Am. Jour. Sci.*, 1973, **273**, 234–251.
10. C. Guo, J. Mao, Bierlein, F.; Z. Chen, Y. Chen, C. Li, Z. Zeng, *Ore Geol. Rev.*, 2011, **43**, 26–39.
11. R. Z. Hu, W. F. Wei, X. W. Bi, J. T. Peng, Y. Q. Qi, L. Y. Wu, Y. W. Chen, *Lithos*, 2012, **150**, 111–118.
12. R. M. Hua,; W. L. Zhang, G. L. Li, Y. Q. Hu, X. D. Wang, *Geol. J. China Univ.*, 2008, **14**, 527–538 (In Chinese with English abstract).
13. M. Harlaux, J. Mercadier, C. Marignac, C. Peiffert, C. Cloquet, M. Cuney, *Chem. Geol.*, 2018b, **479**, 58–85.
14. M. Harlaux, R. L. Romer, J. Mercadier, C. Morlot, C. Marignac, M. Cuney, *Miner. Deposita*, 2018a, **53**, 21–51.
15. D. Jacques, R. Vieira, P. Muchez, M. Sintubin, *Geotect. Res.*, 2015, **97**, 53–55.
16. P. Khavari, *Luleå University of Technology*, 2018, 6–15.
17. H. Legros, M. Harlaux, J. Mercadier, R. L. Romer, M. Poujol, A. Camacho, C. Marignac, M. Cuney, R. C. Wang, N. Charles, M. Y. Lespinasse, *Ore Geol. Rev.* 2020, **117**, 103302.
18. S. T. Li, J. B. Wang, X. Y. Zhu, Y. L. Wang, Y. Hang, N. N. Guo, *Geol. Explor.*, 2011, **47**, 143–150.
19. Q. L. Li, X. H. Li, Z. W. Lan, C. L. Guo, Y. N. Yang, Y. Liu, G. Q. Tang, *Contrib. Mineral. Petrol.*, 2013, **166**, 65–80.
20. X. H. Li, W. X. Li, Z. X. Li, *Chin. Sci. Bull.*, 2007, **52**, 1873–1885.
21. T. Luo, X. D. Deng, J. W. Li, Z. C. Hu, W. Zhang, Y. S. Liu, J. F. Zhang, *J. Anal. At. Spectrom.*, 2019. **34**, 1439–1446.
22. V. Lüders, R. L. Romer, H. A. Gilg, R. J. Bodnar, T. Pettke, D. Misantoni, *Miner. Deposita*, 2009, **44**, 415–434.
23. J. W. Mao, H. Cheng, P. Franco, *Mineral Deposits*. 2013, **48**, 267–294 (In Chinese with English abstract).

24. J. W. Mao, G. Q. Xie, C. L. Guo, Y. C. Chen, *Acta Petrol. Sin.*, 2007, **23**, 2329–2338 (In Chinese with English abstract).
25. R. J. Moscati, L. A. Neymark, *Miner. Deposita*, 2020, **55**, 1–20.
26. L. A. Neymark, C. S. Holm-Denoma, R. J. Moscati, *Chem. Geol.*, 2018, **483**, 410–425.
27. L. G. Ohlsson, *Miner. Deposita*, 1979, **74**, 1012–1034.
28. J. Peng, M. F. Zhou, R. Hu, N. Shen, S. Yuan, X. Bi, A. Du, W. Qu, *Miner. Deposita*, 2006, **41**, 661–669.
29. R. L. Romer, V. Lüders, *Geochim. Cosmochim. Acta*, 2006, **70**, 4725–4733.
30. R. L. Romer, B. Öhlander, *GFF*, 1994, **116**, 161–166.
31. R. L. Romer, S. A. Smeds, *Precambr. Res.*, 1997, **82**, 85–99.
32. E. Seedorff, M. T. Einaudi, *Econ. Geol.*, 2004, **99**, 3–37.
33. W. D. Smith, J. R. Darling, D. S. Bullen, S. Lasalle, I. Pereira, H. Moreira, C. J. Allen, S. Tapster, *Lithos*, 2019, **336,** 14–26.
34. L. W. Snee, J. F. Sutter, W. C. Kelly, *Econ. Geol.*, 1988, **83**, 335–354.
35. T. Sun, *Geol. Bull. China*, 2006, **25**, 232–235 (in Chinese with English abstract).
36. X. Wang, M. Ren, *Ore Geol. Rev.*, 2018, **101**, 453–467.
37. Y. Wang, R. Pei, J. Li, W. Qu, L. Li, H. Wang, A. Du, *Acta Geol. Sin.-English Edition*, 2008, **82**, 820–825.
38. D. H. Wang, H. Q. Li, Y. Qin, Y. P. Mei, Z. H. Chen, W. J. Qu, Y. B. Wang, H. Cai, D. H. Gong, X. P. He, *Rock and Mineral Analysis*, 2009, **28**, 201–208 (In Chinese with English abstract).
39. F. Y. Wang, C. Y. Li, M. X. Ling, H. Zhang, Y. L. Sun, W. D. Sun, *Resource Geol.*, 2011, **61**, 414–423.
40. Y. Zhang, J. H. Yang, J. Y. Chen, H. Wang, Y. X. Xiang, *Lithos*, 2017, **278–281**, 166–180.
41. W. L. Zhang, R. M. Hua, R. C. Wang, L. Xie, X. D. Che, *Mineral Deposits*, 2012, **31**, 633–634 (In Chinese with English abstract).
42. W. W. Zhao, M. F. Zhou, Y. H. M. Li, Z. Zhao, J. F. Gao, *J. Asian Earth Sci.*, 2017, **137**, 109–140.
43. X. M. Zhou, T. Sun, W. Z. Shen, L. S. Shu, Y. L. Niu, *Episodes*, 2006, 29, 26–21.

Electronic Supplementary Material (ESI) for Journal of Analytical Atomic Spectrometry.

Appendix Tables for Supporting Information

Table S1 Major element composition of wolframite samples investigated in this study.

Wolframite	Bagge	Sewa	MTM	Panasqueira	Cornwall	HTD	YGX-2107	YGX-2113	DP-12	XHS16	SHM
	(n=24)	(n=41)	(n=22)	(n=24)	(n=20)	(n=32)	(n=32)	(n=41)	(n=12)	(n=12)	(n=21)
Major element composition (wt%)											
MnO	4.66	6.62	5.95	3.42	4.61	23.90	11.73	13.26	16.87	9.96	23.72
FeO	18.03	17.62	18.20	20.87	19.76	0.19	12.59	10.86	7.56	14.59	0.17
Nb_2O_5	0.37	0.91	0.19	0.20	0.38	0.11	0.42	0.59	0.56	0.68	0.26
Ta_2O_5	0.28	0.15	0.18	0.18	0.24	0.21	0.26	0.30	0.21	0.22	0.26
SnO_2	b.d.	b.d.	b.d.	b.d.	b.d.	0.02	b.d	0.01	0.02	0.01	0.03
WO_3	76.28	75.48	75.35	76.68	76.47	76.39	75.87	75.40	75.61	75.89	76.38
Sc_2O_3	0.04	0.02	0.01	0.01	0.01	0.02	0.02	0.02	0.01	0.08	0.01
TiO_2	0.03	0.03	0.03	0.04	0.03	0.01	0.04	0.02	0.03	0.01	0.05
Total	99.69	100.84	99.91	101.39	101.51	100.85	100.93	100.45	100.88	101.43	100.89
Atoms per unit formula (a.p.u.f.)											
Mn^{2+}	0.1994	0.2794	0.2541	0.1441	0.1938	1.0105	0.4954	0.5623	0.7122	0.4177	1.0018
FeO^T	0.7627	0.7345	0.7680	0.8685	0.8206	0.0079	0.5249	0.4546	0.3151	0.6043	0.0071
Nb^{5+}	0.0085	0.0205	0.0044	0.0044	0.0086	0.0025	0.0094	0.0135	0.0127	0.0152	0.0060
Ta^{5+}	0.0038	0.0020	0.0025	0.0024	0.0032	0.0028	0.0035	0.0041	0.0028	0.0030	0.0035
Sn^{4+}						0.0004		0.0001	0.0004	0.0002	0.0006
W^{6+}	1.0001	0.9751	0.9856	0.9889	0.9843	0.9883	0.9807	0.9785	0.9765	0.9745	0.9870
Sc^{3+}	0.0018	0.0008	0.0005	0.0004	0.0004	0.0007	0.0009	0.0009	0.0005	0.0033	0.0005
Ti^{4+}	0.0012	0.0011	0.0013	0.0014	0.0010	0.0005	0.0014	0.0006	0.0010	0.0002	0.0018
Fe^{2+}	0.7592	0.7328	0.7669	0.8676	0.8197	0.0066	0.5231	0.4528	0.3140	0.5977	0.0060
Fe^{3+}	0.0035	0.0017	0.0011	0.0008	0.0008	0.0013	0.0018	0.0019	0.0011	0.0066	0.0011
Mn/(Fe+Mn)	0.2062	0.2754	0.2486	0.1423	0.1910	0.9923	0.4854	0.5532	0.6934	0.4088	0.9929

Note: n = number of data; b.d. = below detection limit;
Atoms per unit formula are calculated on basis of 4 atoms of oxygen; Fe^{3+} is calculated on the basis of charge balance and 2 cations.

Table S2 Individual LA-SF-ICP-MS U-Pb data of wolframite investigated in this study.

Sample	Pb	Th (μg g^{-1})	U	Th/U	^{238}U /^{206}Pb	1σ	^{207}Pb /^{206}Pb	1σ	^{207}Pb /^{235}U	1σ	^{206}Pb /^{238}U	1σ	Rho	f_{206} [a] (%)	^{207}Pb-corrected (Ma) ^{206}Pb/^{238}U	1σ
Baggetorp W deposit, Sweden (Bagge)																
Bagge-1	2.23	0.30	3.92	0.076	3.08	0.05	0.1016	0.0018	5.47	0.21	0.3245	0.0049	0.40	0.00	1825	32
Bagge-2	3.39	0.64	10.30	0.062	3.07	0.05	0.1326	0.0026	6.09	0.33	0.3253	0.0052	0.29	2.73	1772	34
Bagge-3	2.71	0.37	6.18	0.060	3.07	0.05	0.1467	0.0030	6.30	0.38	0.3259	0.0054	0.28	4.34	1749	35
Bagge-4	3.17	0.62	10.15	0.061	3.12	0.05	0.1116	0.0021	4.94	0.21	0.3205	0.0050	0.36	0.32	1787	32
Bagge-5	3.08	0.55	8.95	0.061	3.10	0.05	0.1202	0.0021	5.39	0.21	0.3223	0.0049	0.40	1.30	1780	32
Bagge-6	3.82	0.71	10.50	0.068	3.07	0.05	0.1280	0.0029	6.42	0.45	0.3256	0.0055	0.24	2.20	1782	35
Bagge-7	3.32	0.90	11.50	0.078	3.13	0.05	0.1093	0.0024	4.71	0.29	0.3198	0.0053	0.27	0.06	1788	34
Bagge-8	1.86	0.06	5.52	0.010	3.09	0.06	0.1128	0.0036	4.81	0.50	0.3236	0.0066	0.19	0.46	1800	42
Bagge-9	2.06	21.02	9.94	2.115	3.13	0.05	0.1048	0.0024	4.63	0.29	0.3199	0.0053	0.27	0.00	1797	34
Bagge-10	1.81	0.07	6.13	0.012	3.04	0.07	0.1449	0.0050	7.25	0.98	0.3290	0.0075	0.17	5.35	1748	48
Bagge-11	2.16	0.10	7.77	0.010	3.12	0.05	0.1016	0.0020	4.56	0.23	0.3207	0.0051	0.32	0.33	1788	33
Bagge-12	1.25	0.01	4.41	0.001	3.12	0.06	0.0983	0.0030	4.65	0.49	0.3204	0.0063	0.18	0.00	1793	40
Rwanda (Sewa)																
Sewa-1	1.79	0.29	14.11	0.021	7.57	0.12	0.0751	0.0019	1.36	0.06	0.1321	0.0021	0.35	1.16	791.2	13.3
Sewa-2	3.04	0.41	23.77	0.017	7.53	0.11	0.0757	0.0016	1.40	0.04	0.1328	0.0020	0.47	1.24	794.5	12.6
Sewa-3	3.45	0.48	27.65	0.017	7.60	0.11	0.0692	0.0015	1.25	0.04	0.1315	0.0019	0.46	0.45	793.2	12.5
Sewa-4	3.38	0.48	23.26	0.021	7.36	0.11	0.1024	0.0020	1.88	0.05	0.1359	0.0020	0.51	4.47	787.1	12.8
Sewa-5	4.76	0.38	18.74	0.020	7.58	0.12	0.0691	0.0019	1.32	0.07	0.1319	0.0021	0.32	0.43	795.4	13.6
Sewa-6	2.51	0.38	18.86	0.020	7.51	0.11	0.0821	0.0019	1.50	0.06	0.1332	0.0020	0.39	2.00	790.9	13.0
Sewa-7	2.36	0.52	18.83	0.028	7.58	0.11	0.0730	0.0017	1.34	0.05	0.1319	0.0020	0.38	0.91	791.7	12.9
Sewa-8	2.41	0.57	16.38	0.035	7.25	0.11	0.1104	0.0023	2.11	0.08	0.1380	0.0021	0.40	5.43	790.8	13.3
Sewa-9	2.04	0.36	16.01	0.022	7.59	0.11	0.0732	0.0016	1.28	0.05	0.1317	0.0020	0.41	0.93	790.4	12.6
Sewa-10	*2.67*	*0.48*	*13.83*	*0.034*	*6.76*	*0.10*	*0.1757*	*0.0034*	*3.54*	*0.12*	*0.1479*	*0.0022*	*0.44*	*13.3*	*777.5*	*14.0*
Sewa-11	3.27	0.37	21.39	0.017	7.25	0.10	0.1114	0.0021	2.14	0.06	0.1379	0.0020	0.51	5.56	789.1	12.8
Sewa-12	2.63	0.31	18.75	0.017	7.43	0.11	0.0911	0.0018	1.68	0.05	0.1347	0.0019	0.48	3.10	790.6	12.5
Sewa-13	*4.07*	*0.30*	*18.48*	*0.016*	*6.45*	*0.09*	*0.2121*	*0.0039*	*4.42*	*0.14*	*0.1550*	*0.0023*	*0.46*	*17.7*	*773.5*	*14.5*
Sewa-14	*3.25*	*0.19*	*10.63*	*0.018*	*6.31*	*0.10*	*0.2268*	*0.0050*	*4.96*	*0.27*	*0.1585*	*0.0026*	*0.30*	*19.5*	*773.7*	*16.6*
Sewa-15	3.30	0.45	25.61	0.018	7.63	0.11	0.0686	0.0015	1.23	0.04	0.1310	0.0019	0.41	0.37	790.8	12.4
Sewa-16	4.81	0.58	31.78	0.018	7.36	0.10	0.0965	0.0018	1.83	0.05	0.1358	0.0019	0.55	3.75	792.0	12.3
Sewa-17	4.74	0.61	35.10	0.017	7.57	0.11	0.0745	0.0017	1.35	0.05	0.1322	0.0020	0.39	1.09	792.0	12.6
Sewa-18	4.55	0.51	28.87	0.018	7.28	0.10	0.1056	0.0020	2.04	0.06	0.1374	0.0020	0.47	4.86	791.8	12.7
Sewa-19	*4.78*	*0.50*	*28.60*	*0.018*	*6.96*	*0.10*	*0.1492*	*0.0028*	*2.94*	*0.09*	*0.1438*	*0.0021*	*0.45*	*10.1*	*783.3*	*13.3*
Sewa-20	3.57	0.45	16.17	0.028	7.31	0.11	0.1012	0.0024	2.00	0.10	0.1368	0.0021	0.32	4.32	793.0	13.7
Sewa-21	*2.75*	*0.35*	*15.56*	*0.022*	*6.92*	*0.10*	*0.1511*	*0.0032*	*3.06*	*0.13*	*0.1446*	*0.0022*	*0.36*	*10.4*	*785.5*	*14.1*

Table S2 (continued)

Sample	Pb	Th ($\mu g\ g^{-1}$)	U	Th/U	$^{238}U/^{206}Pb$	1σ	$^{207}Pb/^{206}Pb$	1σ	$^{207}Pb/^{235}U$	1σ	$^{206}Pb/^{238}U$	1σ	Rho	f_{206} [a] (%)	^{207}Pb-corrected (Ma) $^{206}Pb/^{238}U$	1σ
Les Montmins, France (MTM)																
MTM-1	2.49	0.04	43.90	0.001	18.80	0.33	0.0617	0.0019	0.439	0.018	0.0532	0.0009	0.42	1.06	330.6	5.9
MTM-2	1.70	0.02	36.60	0.001	18.88	0.32	0.0554	0.0019	0.391	0.017	0.0530	0.0009	0.40	0.29	331.8	5.9
MTM-3	2.05	0.08	39.30	0.002	18.81	0.38	0.0517	0.0025	0.376	0.025	0.0532	0.0011	0.31	0.00	334.5	7.0
MTM-4	1.35	0.01	31.34	0.000	18.59	0.39	0.0529	0.0026	0.389	0.028	0.0538	0.0011	0.30	0.00	337.9	7.3
MTM-5	0.96	0.01	21.18	0.000	18.94	0.38	0.0520	0.0024	0.376	0.024	0.0528	0.0011	0.32	0.00	332.2	6.8
MTM-6	0.74	0.01	16.72	0.000	18.83	0.50	0.0512	0.0038	0.389	0.041	0.0531	0.0014	0.25	0.00	334.3	9.0
MTM-7	0.90	0.01	19.42	0.000	18.73	0.37	0.0495	0.0023	0.374	0.024	0.0534	0.0011	0.31	0.00	336.7	6.8
MTM-8	0.96	0.01	21.28	0.001	19.02	0.38	0.0499	0.0024	0.355	0.023	0.0526	0.0010	0.31	0.00	331.6	6.7
MTM-9	1.47	0.02	30.70	0.001	18.85	0.33	0.0498	0.0018	0.368	0.017	0.0531	0.0009	0.38	0.00	334.6	6.0
MTM-10	1.98	0.04	44.80	0.001	18.85	0.32	0.0498	0.0018	0.368	0.017	0.0530	0.0009	0.36	0.00	334.5	5.9
MTM-11	1.58	0.03	35.40	0.001	18.81	0.37	0.0529	0.0024	0.393	0.025	0.0532	0.0011	0.31	0.00	334.0	6.8
MTM-12	0.91	0.01	20.46	0.001	18.61	0.51	0.0494	0.0040	0.380	0.044	0.0537	0.0015	0.24	0.00	338.9	9.5
MTM-13	0.83	0.01	18.39	0.001	18.72	0.38	0.0518	0.0025	0.365	0.024	0.0534	0.0011	0.31	0.00	336.1	7.0
MTM-14	1.89	0.04	40.70	0.001	18.85	0.33	0.0624	0.0022	0.437	0.021	0.0530	0.0009	0.37	1.16	329.4	6.0
MTM-15	0.76	0.01	17.03	0.000	18.52	0.81	0.0523	0.0070	0.390	0.073	0.0540	0.0024	0.23	0.00	339.4	15.3
MTM-16	0.75	0.01	16.88	0.000	18.87	0.40	0.0513	0.0027	0.373	0.028	0.0530	0.0011	0.29	0.00	333.6	7.2
Yaogangxian W deposit, Hunan Province, China (YGX-2107)																
YGX-2107-1	0.89	0.59	39.90	0.015	39.17	0.66	0.0491	0.0017	0.171	0.007	0.02553	0.00043	0.44	0.00	162.5	2.8
YGX-2107-2	0.42	0.23	17.40	0.013	39.68	0.85	0.0525	0.0030	0.177	0.012	0.02520	0.00054	0.32	0.42	159.8	3.5
YGX-2107-3	0.59	0.19	25.51	0.008	39.20	0.66	0.0498	0.0019	0.174	0.007	0.02551	0.00043	0.41	0.08	162.3	2.8
YGX-2107-4	0.83	0.23	37.63	0.006	38.79	0.63	0.0482	0.0015	0.168	0.006	0.02578	0.00042	0.47	0.00	164.3	2.7
YGX-2107-5	1.24	1.00	45.60	0.022	39.97	0.70	0.0500	0.0025	0.172	0.009	0.02502	0.00044	0.32	0.11	159.1	2.8
YGX-2107-6	0.43	0.21	17.67	0.012	39.05	0.73	0.0474	0.0023	0.168	0.009	0.02561	0.00048	0.35	0.00	163.4	3.1
YGX-2107-7	0.15	0.07	6.30	0.011	39.28	0.93	0.0477	0.0038	0.169	0.015	0.02546	0.00060	0.26	0.00	162.4	3.9
YGX-2107-8	0.16	0.15	7.33	0.021	39.78	1.80	0.0448	0.0090	0.171	0.040	0.02514	0.00114	0.19	0.00	160.9	7.3
YGX-2107-9	0.49	0.59	22.00	0.027	38.88	1.21	0.0495	0.0049	0.171	0.020	0.02572	0.00080	0.26	0.04	163.6	5.2
YGX-2107-10	0.34	0.35	14.23	0.025	40.19	0.97	0.0528	0.0037	0.181	0.015	0.02488	0.00060	0.29	0.46	157.7	3.9
YGX-2107-11	0.49	0.39	21.25	0.018	39.81	2.04	0.0578	0.0090	0.182	0.035	0.02512	0.00129	0.27	1.08	158.2	8.3
YGX-2107-12	0.41	0.35	17.48	0.020	39.53	0.70	0.0487	0.0020	0.168	0.008	0.02530	0.00045	0.38	0.00	161.2	2.9
YGX-2107-13	1.59	1.19	67.40	0.018	39.98	0.83	0.0500	0.0026	0.180	0.011	0.02501	0.00052	0.33	0.10	159.1	3.4
YGX-2107-14	3.46	1.60	151.80	0.011	39.17	0.58	0.0471	0.0009	0.171	0.004	0.02553	0.00038	0.71	0.00	162.9	2.4
YGX-2107-15	0.26	0.14	10.60	0.013	39.87	1.86	0.0516	0.0079	0.175	0.032	0.02508	0.00117	0.25	0.31	159.2	7.5
YGX-2107-16	0.16	0.11	6.94	0.016	39.57	1.30	0.0507	0.0054	0.168	0.021	0.02527	0.00083	0.26	0.20	160.6	5.3
YGX-2107-17	0.93	0.48	40.90	0.012	39.42	1.35	0.0546	0.0056	0.182	0.023	0.02537	0.00087	0.27	0.68	160.4	5.6

Table S2 (continued)

Sample	Pb	Th	U	Th/U	$^{238}U/^{206}Pb$	1σ	$^{207}Pb/^{206}Pb$	1σ	$^{207}Pb/^{235}U$	1σ	$^{206}Pb/^{238}U$	1σ	Rho	f_{206} [a]	^{207}Pb-corrected (Ma)	
		(μg g^{-1})												(%)	$^{206}Pb/^{238}U$	1σ
YGX-2107-18	0.67	0.37	29.00	0.013	39.48	0.65	0.0498	0.0017	0.174	0.006	0.02533	0.00042	0.44	0.08	161.1	2.7
YGX-2107-19	1.02	1.33	44.90	0.030	40.14	0.81	0.0535	0.0026	0.182	0.011	0.02491	0.00050	0.34	0.55	157.8	3.2
Xihuashan W deposit, Jiangxi Province, China (XHS16)																
XHS16-1	0.36	0.25	15.35	0.016	39.56	0.72	0.0500	0.0021	0.177	0.008	0.02528	0.00046	0.39	0.09	160.8	3.0
XHS16-2	0.23	0.16	9.47	0.016	39.49	1.05	0.0511	0.0038	0.174	0.015	0.02532	0.00067	0.30	0.23	160.8	4.3
XHS16-3	0.46	0.33	20.40	0.016	39.56	0.80	0.0472	0.0023	0.167	0.009	0.02528	0.00051	0.36	0.00	161.4	3.3
XHS16-4	0.40	0.28	17.42	0.016	39.28	0.76	0.0459	0.0021	0.166	0.009	0.02546	0.00049	0.36	0.00	162.7	3.2
XHS16-5	0.84	0.64	38.02	0.017	39.48	0.70	0.0505	0.0018	0.175	0.007	0.02533	0.00045	0.44	0.15	161.0	2.9
XHS16-6	0.15	0.09	6.21	0.015	40.23	2.62	0.0535	0.0121	0.176	0.048	0.02486	0.00162	0.24	0.53	157.5	10.4
XHS16-7	0.10	0.08	4.59	0.018	39.71	1.17	0.0524	0.0050	0.175	0.019	0.02518	0.00074	0.27	0.39	159.7	4.8
XHS16-8	0.16	0.14	6.54	0.021	39.51	2.45	0.0650	0.0119	0.188	0.041	0.02531	0.00157	0.29	1.98	158.0	10.1
XHS16-9	0.13	0.17	5.21	0.032	38.87	2.93	0.0571	0.0141	0.180	0.052	0.02573	0.00194	0.26	0.98	162.2	12.5
XHS16-10	0.09	0.06	3.85	0.015	39.76	1.08	0.0522	0.0051	0.178	0.019	0.02515	0.00068	0.25	0.37	159.5	4.4
XHS16-11	0.14	0.10	6.10	0.016	38.94	1.20	0.0523	0.0050	0.182	0.020	0.02568	0.00079	0.28	0.38	162.8	5.1
XHS16-12	0.17	0.14	7.41	0.019	39.67	0.91	0.0536	0.0035	0.181	0.014	0.02521	0.00058	0.31	0.54	159.6	3.7
XHS16-13	0.31	0.10	12.28	0.008	39.14	0.83	0.0485	0.0027	0.175	0.011	0.02555	0.00054	0.33	0.00	162.8	3.5
XHS16-14	0.17	0.13	7.68	0.016	39.31	1.14	0.0505	0.0043	0.171	0.017	0.02544	0.00074	0.29	0.15	161.7	4.8
XHS16-15	0.20	0.14	8.64	0.017	39.62	0.83	0.0516	0.0027	0.178	0.011	0.02524	0.00053	0.35	0.29	160.2	3.4
XHS16-16	0.24	0.18	10.92	0.016	39.32	0.96	0.0516	0.0035	0.182	0.014	0.02543	0.00062	0.31	0.29	161.4	4.0
XHS16-17	0.05	0.03	2.33	0.014	39.60	1.52	0.0547	0.0083	0.176	0.029	0.02525	0.00097	0.23	0.69	159.7	6.2
XHS16-18	0.12	0.11	4.57	0.025	39.79	1.66	0.0500	0.0078	0.181	0.033	0.02513	0.00105	0.23	0.10	159.8	6.8
XHS16-19	0.23	0.18	9.63	0.019	38.77	1.58	0.0522	0.0066	0.186	0.028	0.02579	0.00105	0.27	0.37	163.5	6.8
XHS16-20	0.20	0.15	8.22	0.018	39.71	0.90	0.0552	0.0034	0.187	0.013	0.02518	0.00057	0.32	0.74	159.1	3.7
Dangping W deposit, Jiangxi Province, China (DP-12)																
DP-12-1	1.26	0.78	55.20	0.014	39.90	0.65	0.0509	0.0014	0.182	0.005	0.02506	0.00041	0.54	0.21	159.2	2.6
DP-12-2	1.31	0.83	59.70	0.014	39.34	0.77	0.0463	0.0021	0.169	0.009	0.02542	0.00050	0.38	0.00	162.4	3.2
DP-12-3	0.52	0.27	22.28	0.012	40.39	0.73	0.0503	0.0019	0.177	0.007	0.02476	0.00045	0.43	0.13	157.5	2.9
DP-12-4	0.41	0.19	18.46	0.010	38.94	0.99	0.0461	0.0034	0.171	0.014	0.02568	0.00065	0.30	0.00	164.1	4.2
DP-12-5	0.53	0.19	23.64	0.008	39.49	1.20	0.0458	0.0041	0.170	0.018	0.02532	0.00077	0.29	0.00	161.9	5.0
DP-12-6	0.44	0.24	19.25	0.012	39.76	0.82	0.0506	0.0024	0.183	0.010	0.02515	0.00052	0.37	0.17	159.9	3.4
DP-12-7	1.43	0.52	62.80	0.008	39.82	0.65	0.0510	0.0013	0.183	0.005	0.02511	0.00041	0.58	0.22	159.5	2.6
DP-12-8	1.19	0.36	42.00	0.009	38.79	1.11	0.0522	0.0041	0.175	0.016	0.02578	0.00074	0.31	0.37	163.5	4.8
DP-12-9	1.99	0.70	83.40	0.008	39.81	0.65	0.0483	0.0011	0.174	0.005	0.02512	0.00041	0.62	0.00	160.1	2.6
DP-12-10	0.84	0.27	37.80	0.007	39.48	0.69	0.0486	0.0015	0.170	0.006	0.02533	0.00044	0.49	0.00	161.4	2.8
DP-12-11	0.78	0.27	34.20	0.008	40.52	0.79	0.0536	0.0022	0.178	0.008	0.02468	0.00048	0.42	0.55	156.3	3.1

Table S2 (continued)

Sample	Pb	Th	U	Th/U	$^{238}U/^{206}Pb$	1σ	$^{207}Pb/^{206}Pb$	1σ	$^{207}Pb/^{235}U$	1σ	$^{206}Pb/^{238}U$	1σ	Rho	f_{206} [a]	^{207}Pb-corrected (Ma)	
		(μg g^{-1})												(%)	$^{206}Pb/^{238}U$	1σ
DP-12-12	0.52	0.18	21.21	0.008	39.09	1.25	0.0544	0.0049	0.180	0.019	0.02558	0.00082	0.30	0.64	161.8	5.3
DP-12-13	0.67	0.28	29.80	0.009	40.16	0.97	0.0496	0.0030	0.179	0.013	0.02490	0.00060	0.33	0.05	158.5	3.9
DP-12-14	2.81	0.91	125.80	0.007	39.37	0.62	0.0484	0.0010	0.171	0.004	0.02540	0.00040	0.68	0.00	161.9	2.6
DP-12-15	2.00	0.58	84.70	0.007	40.02	0.64	0.0490	0.0011	0.170	0.004	0.02499	0.00040	0.65	0.00	159.2	2.6
DP-12-16	2.75	0.84	125.90	0.007	39.14	0.63	0.0464	0.0011	0.166	0.004	0.02555	0.00041	0.64	0.00	163.2	2.6
DP-12-17	0.36	0.17	16.57	0.010	38.31	0.88	0.0484	0.0029	0.172	0.012	0.02610	0.00060	0.33	0.00	166.3	3.9
DP-12-18	0.96	0.40	43.10	0.009	38.71	0.69	0.0462	0.0015	0.166	0.006	0.02583	0.00046	0.47	0.00	165.0	3.0
DP-12-19	5.33	2.20	250.10	0.009	38.52	0.61	0.0456	0.0009	0.167	0.004	0.02596	0.00041	0.70	0.00	166.0	2.6
Panasqueira W-Sn-Cu deposit, Portugal (Panasqueira)																
Panasqueira-1	0.07	0.00	1.56	0.003	19.83	1.07	0.0422	0.0076	0.361	0.089	0.0504	0.0027	0.22	0.00	321.1	17.4
Panasqueira-2	0.06	0.00	1.38	0.002	19.62	1.02	0.0507	0.0077	0.351	0.074	0.0510	0.0026	0.25	0.00	321.2	17.0
Panasqueira-3	0.12	0.01	2.07	0.003	19.53	0.65	0.0582	0.0051	0.359	0.042	0.0512	0.0017	0.29	0.70	319.7	11.0
Panasqueira-4	0.08	0.00	1.71	0.002	20.08	0.69	0.0527	0.0053	0.363	0.052	0.0498	0.0017	0.24	0.01	313.3	10.9
Panasqueira-5	0.35	0.01	4.02	0.003	19.76	0.71	0.0519	0.0049	0.347	0.047	0.0506	0.0018	0.27	0.00	318.5	11.7
Panasqueira-6	0.09	0.01	2.07	0.002	19.90	1.40	0.0616	0.0122	0.368	0.099	0.0502	0.0035	0.26	1.13	312.5	22.8
Panasqueira-7	0.09	0.00	2.06	0.001	20.10	1.20	0.0569	0.0095	0.356	0.083	0.0498	0.0030	0.26	0.54	311.3	19.2
Panasqueira-8	0.07	0.00	1.46	0.002	20.15	0.64	0.0600	0.0063	0.373	0.047	0.0496	0.0016	0.25	0.93	309.4	10.2
Panasqueira-9	0.20	0.00	4.64	0.001	19.49	1.22	0.0450	0.0089	0.350	0.104	0.0513	0.0032	0.21	0.00	325.5	20.7
Panasqueira-10	0.20	0.00	4.51	0.001	20.10	0.62	0.0512	0.0043	0.356	0.042	0.0498	0.0015	0.26	0.00	313.5	9.9
Panasqueira-11	0.16	0.01	3.63	0.002	20.42	0.70	0.0503	0.0049	0.359	0.052	0.0490	0.0017	0.24	0.00	309.1	10.8
Panasqueira-12	0.08	0.00	1.90	0.001	19.94	0.95	0.0523	0.0078	0.357	0.076	0.0501	0.0024	0.22	0.00	315.5	15.5
Panasqueira-13	0.02	0.00	0.52	0.003	20.70	1.47	0.0504	0.0192	0.350	0.169	0.0483	0.0034	0.15	0.00	305.0	22.1
Panasqueira-14	0.09	0.00	2.11	0.001	19.94	0.84	0.0458	0.0072	0.352	0.080	0.0501	0.0021	0.19	0.00	318.0	13.6
Panasqueira-15	0.06	0.00	1.44	0.001	20.32	1.23	0.0611	0.0111	0.367	0.097	0.0492	0.0030	0.23	1.06	306.5	19.2
Panasqueira-16	0.09	0.00	2.07	0.001	20.42	0.87	0.0524	0.0073	0.350	0.069	0.0490	0.0021	0.21	0.00	308.2	13.4
Panasqueira-17	0.08	0.00	1.30	0.003	22.10	1.54	0.0635	0.0152	0.359	0.113	0.0452	0.0032	0.22	1.36	281.4	20.3
Cornwall W-Sn deposit, United Kingdom (Cornwall)																
Cornwall-1	0.48	0.12	11.41	0.011	21.96	0.82	0.0691	0.0075	0.354	0.057	0.0455	0.0017	0.23	2.15	281.0	10.9
Cornwall-2	0.79	0.17	18.50	0.009	22.16	0.60	0.0538	0.0053	0.305	0.040	0.0451	0.0012	0.21	0.24	283.8	7.9
Cornwall-3	0.80	0.16	18.32	0.009	22.25	0.50	0.0581	0.0041	0.341	0.034	0.0449	0.0010	0.23	0.78	281.2	6.5
Cornwall-4	0.51	0.11	12.21	0.009	22.22	0.60	0.0592	0.0048	0.328	0.038	0.0450	0.0012	0.23	0.92	281.3	7.9
Cornwall-5	0.55	0.13	12.98	0.010	22.24	0.40	0.0591	0.0026	0.349	0.021	0.0450	0.0008	0.30	0.90	281.0	5.2
Cornwall-6	0.58	0.14	14.08	0.010	22.04	0.46	0.0551	0.0031	0.356	0.029	0.0454	0.0010	0.26	0.41	284.9	6.1
Cornwall-7	0.58	0.13	13.90	0.009	22.24	0.42	0.0559	0.0026	0.327	0.020	0.0450	0.0009	0.30	0.50	282.2	5.5
Cornwall-8	0.51	0.11	11.92	0.009	22.24	0.38	0.0565	0.0022	0.347	0.018	0.0450	0.0008	0.34	0.57	282.0	5.0

Table S2 (continued)

Sample	Pb	Th	U	Th/U	$^{238}U/^{206}Pb$	1σ	$^{207}Pb/^{206}Pb$	1σ	$^{207}Pb/^{235}U$	1σ	$^{206}Pb/^{238}U$	1σ	Rho	f_{206} [a]	^{207}Pb-corrected (Ma)	
		(μg g^{-1})												(%)	$^{206}Pb/^{238}U$	1σ
Cornwall-9	0.56	0.13	13.19	0.009	22.09	0.40	0.0550	0.0028	0.335	0.022	0.0453	0.0008	0.28	0.39	284.3	5.3
Cornwall-10	0.56	0.13	13.74	0.009	22.15	0.49	0.0523	0.0031	0.320	0.025	0.0451	0.0010	0.28	0.05	284.5	6.4
Cornwall-11	0.81	0.16	19.19	0.008	21.78	0.41	0.0517	0.0024	0.332	0.020	0.0459	0.0009	0.31	0.00	289.4	5.6
Cornwall-12	0.44	0.11	10.66	0.010	22.10	0.43	0.0534	0.0022	0.338	0.018	0.0453	0.0009	0.36	0.18	284.8	5.7
Cornwall-13	0.55	0.11	10.83	0.010	21.86	0.45	0.0515	0.0023	0.328	0.019	0.0457	0.0009	0.36	0.00	288.4	6.1
Cornwall-14	0.50	0.11	12.20	0.009	21.30	0.46	0.0457	0.0022	0.302	0.019	0.0470	0.0010	0.34	0.00	298.0	6.5
Cornwall-15	0.58	0.12	12.32	0.010	22.21	0.57	0.0604	0.0035	0.377	0.030	0.0450	0.0012	0.32	1.06	281.0	7.4
Cornwall-16	3.83	0.13	13.18	0.010	21.39	0.46	0.0472	0.0022	0.307	0.018	0.0468	0.0010	0.36	0.00	296.3	6.5
Hamme tungsten district, United States (HTD)																
HTD-1	0.11	0.01	2.20	0.003	21.99	0.58	0.0784	0.0062	0.436	0.043	0.0455	0.0012	0.27	3.31	277.4	7.8
HTD-2	0.77	0.01	17.24	0.000	22.19	0.35	0.0521	0.0016	0.330	0.013	0.0451	0.0007	0.41	0.03	284.1	4.6
HTD-3	0.36	0.01	8.07	0.001	22.17	0.40	0.0575	0.0025	0.354	0.020	0.0451	0.0008	0.32	0.70	282.5	5.3
HTD-4	0.34	0.00	7.52	0.001	22.23	0.40	0.0534	0.0022	0.325	0.017	0.0450	0.0008	0.33	0.18	283.1	5.2
HTD-5	0.44	0.01	10.20	0.001	22.20	0.38	0.0568	0.0022	0.351	0.017	0.0451	0.0008	0.35	0.62	282.3	5.0
HTD-6	0.19	0.01	3.60	0.003	21.80	0.47	0.0832	0.0042	0.499	0.035	0.0459	0.0010	0.31	3.90	278.1	6.3
HTD-7	0.13	0.01	2.57	0.002	21.85	0.52	0.0812	0.0051	0.491	0.042	0.0458	0.0011	0.28	3.65	278.2	7.0
HTD-8	0.17	0.01	3.55	0.002	22.09	0.50	0.0675	0.0042	0.415	0.034	0.0453	0.0010	0.28	1.95	280.0	6.6
HTD-9	2.50	0.03	59.50	0.000	22.27	0.33	0.0540	0.0012	0.326	0.008	0.0449	0.0007	0.61	0.26	282.4	4.3
HTD-10	2.28	0.03	53.40	0.001	22.36	0.33	0.0525	0.0011	0.320	0.008	0.0447	0.0007	0.60	0.08	281.8	4.2
HTD-11	1.63	0.02	39.20	0.000	22.29	0.33	0.0528	0.0013	0.320	0.009	0.0449	0.0007	0.53	0.11	282.6	4.3
HTD-12	0.25	0.00	5.74	0.001	22.24	0.43	0.0577	0.0029	0.342	0.022	0.0450	0.0009	0.30	0.72	281.6	5.6
HTD-13	0.14	0.00	3.10	0.001	22.17	0.51	0.0676	0.0043	0.380	0.031	0.0451	0.0010	0.28	1.96	279.0	6.7
HTD-14	0.50	0.01	11.66	0.001	22.25	0.38	0.0593	0.0022	0.351	0.016	0.0449	0.0008	0.37	0.93	280.8	5.0
HTD-15	0.20	0.02	4.23	0.004	21.82	0.45	0.0760	0.0039	0.471	0.032	0.0458	0.0010	0.30	3.01	280.3	6.1
HTD-16	0.30	0.01	6.08	0.002	21.89	0.43	0.0806	0.0035	0.486	0.028	0.0457	0.0009	0.34	3.57	277.9	5.8
HTD-17	0.26	0.01	5.65	0.001	22.17	0.44	0.0654	0.0031	0.374	0.023	0.0451	0.0009	0.32	1.68	279.8	5.8
HTD-18	0.40	0.01	9.25	0.001	22.18	0.39	0.0630	0.0024	0.368	0.018	0.0451	0.0008	0.37	1.39	280.4	5.2
Sweet Home Mine, United States (SHM)																
SHM-1	0.11	0.03	23.63	0.001	251.3	9.5	0.0542	0.0078	0.0299	0.0043	0.00398	0.00015	0.26	0.96	25.4	1.0
SHM-2	0.06	0.14	12.96	0.010	240.4	9.2	0.0781	0.0111	0.0456	0.0064	0.00416	0.00016	0.27	3.99	25.7	1.0
SHM-3	0.14	0.06	34.70	0.002	251.3	6.3	0.0529	0.0039	0.0299	0.0022	0.00398	0.00010	0.34	0.81	25.4	0.6
SHM-4	0.25	0.07	65.10	0.001	253.2	5.8	0.0461	0.0033	0.0258	0.0018	0.00395	0.00009	0.32	0.00	25.4	0.6
SHM-5	0.11	0.04	25.94	0.002	246.9	7.9	0.0543	0.0065	0.0313	0.0038	0.00405	0.00013	0.27	0.99	25.8	0.8
SHM-6	0.07	0.02	18.21	0.001	246.9	7.3	0.0585	0.0066	0.0336	0.0038	0.00405	0.00012	0.26	1.52	25.7	0.8
SHM-7	0.15	0.49	36.62	0.013	242.7	5.3	0.0623	0.0043	0.0362	0.0025	0.00412	0.00009	0.32	1.99	26.0	0.6

Table S2 (continued)

Sample	Pb	Th	U	Th/U	$^{238}U/^{206}Pb$	1σ	$^{207}Pb/^{206}Pb$	1σ	$^{207}Pb/^{235}U$	1σ	$^{206}Pb/^{238}U$	1σ	Rho	f_{206} [a]	^{207}Pb-corrected (Ma)	
		(μg g^{-1})												(%)	$^{206}Pb/^{238}U$	1σ
SHM-8	0.09	0.03	20.71	0.002	243.3	7.7	0.0629	0.0060	0.0355	0.0034	0.00411	0.00013	0.33	2.06	25.9	0.8
SHM-9	0.07	0.02	16.84	0.001	246.3	7.9	0.0604	0.0070	0.0340	0.0039	0.00406	0.00013	0.28	1.75	25.7	0.8
SHM-10	0.09	0.03	22.95	0.001	250.6	8.2	0.0521	0.0066	0.0284	0.0036	0.00399	0.00013	0.26	0.70	25.5	0.8
SHM-11	0.07	0.03	17.42	0.002	254.5	8.4	0.0465	0.0076	0.0257	0.0042	0.00393	0.00013	0.20	0.00	25.3	0.8
SHM-12	0.14	0.08	31.38	0.002	251.9	9.5	0.0526	0.0074	0.0295	0.0041	0.00397	0.00015	0.27	0.76	25.3	1.0
SHM-13	0.31	0.22	79.80	0.003	243.9	4.8	0.0444	0.0022	0.0258	0.0013	0.00410	0.00008	0.39	0.00	26.4	0.5
SHM-14	0.37	0.46	90.30	0.005	249.4	5.0	0.0602	0.0025	0.0339	0.0014	0.00401	0.00008	0.48	1.73	25.4	0.5

[a] f_{206}, common ^{206}Pb in total ^{206}Pb; $f_{206} = [(^{207}Pb/^{206}Pb)\text{total} - (^{207}Pb/^{206}Pb)\text{radiogenic}] / [(^{207}Pb/^{206}Pb)\text{init} - (^{207}Pb/^{206}Pb)\text{radiogenic}]$;

[b] Values shown in italics have not been used to calculate average values shown in Table 4.

Table S3 ID-TIMS U-Pb data shown in Fig. 2d.

Sample	$^{238}U/^{204}Pb$	$^{206}Pb/^{204}Pb$	$^{207}Pb/^{204}Pb$
YGX-2107, Hunan Province, China			
7Y1	36500	928	60.6
7Y2	15400	412	34.9
7Y3	60200	1510	92.4
7Y4	29000	766	52.5
7Y5	26800	719	50.3
7Y6	23600	640	46.5

Isotope ratios not shown in Table 3, but used in Fig. 2d to estimate initial Pb isotopic composition.

Isotope ratios corrected for fractionation, blank, isotopic tracer, 15 pg Pb and 1 pg U blank.